Evaluating Microphysics, Cumulus, and Lightning Parameterization Schemes in WRF Model for Thunderstorm Simulation Over East India

A Thesis

submitted to

Indian Institute of Science Education and Research Pune in partial fulfilment of the requirements for the BS-MS Dual Degree Programme

by

Rinuragavi V N

Indian Institute of Science Education and Research Pune
Dr. Homi Bhabha Road,
Pashan, Pune 411008, INDIA.

April, 2025

Supervisor: Dr. Sunil D Pawar
Indian Institute of Tropical Meteorology, Pune

CERTIFICATE

This is to certify that this dissertation entitled "Evaluating Microphysics, Cumulus, and Lightning Parameterization Schemes in WRF Model for Thunderstorm Simulation Over East India" towards the partial fulfilment of the BS-MS dual degree programme at the Indian Institute of Science Education and Research, Pune represents study/work carried out by Rinuragavi V N at Indian Institute of Tropical Meteorology (IITM), Pune under the supervision of Dr. Sunil D Pawar, Scientist G, Thunderstorm Dynamics, during the academic year 2024-2025.

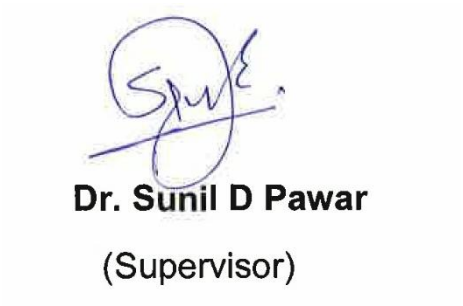

Dr. Sunil D Pawar

(Supervisor)

Rinuragavi V N

(ID: 20201240)

Dedicated to

my Family and Friends

DECLARATION

I hereby declare that the matter embodied in the report entitled "Evaluating Microphysics, Cumulus, and Lightning Parameterization Schemes in WRF Model for Thunderstorm Simulation Over East India" are the results of the work carried out by me at the Department of Earth and Climate Science, Indian Institute of Science Education & Research (IISER) Pune, under the supervision of Dr. Sunil D Pawar, and the same has not been submitted elsewhere for any other degree. Wherever others contribute, every effort is made to indicate this clearly, with due reference to the literature and acknowledgement of collaborative research and discussions.

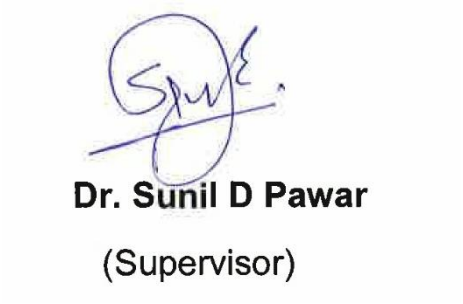

Dr. Sunil D Pawar

(Supervisor)

Rinuragavi V N

(ID: 20201240)

Acknowledgment

I would like to express my sincere gratitude to my Supervisor, Dr. Sunil D. Pawar, Scientist G at the Indian Institute of Tropical Meteorology (IITM), Pune, for his constant guidance throughout my project. I deeply appreciate the freedom he provided me to explore and implement my ideas, which greatly enriched my research experience.

I am especially thankful to Dr. Rupraj Biswasharma, Scientist B at IITM Pune, for his unwavering support, encouragement, and insightful guidance. His scientific expertise has profoundly helped in improving the quality of my research.

I would also like to thank Dr. Umakanth Nandivada, Research Associate at IITM Pune, for his patience and thorough teaching of the WRF model, from installation to execution. His support was instrumental in simplifying the technical aspects of the project, and his constant encouragement has helped me develop new skills and expand my knowledge.

I thank Mr. Manoj Arjun Domkawale, Scientist B at IITM Pune, for his help in sharing the ILLN sensor data.

I sincerely acknowledge IITM Pune for granting me the access to the HPC facility (PRATYUSH), which was essential for running the WRF model.

I am grateful to my family and friends for their continuous love and encouragement which has been a constant source of motivation throughout this journey.

Rinuragavi V N

TABLE OF CONTENTS

TABLES:

FIGURES:

ABSTRACT

Lightning are the electrical discharges that result from non-inductive charging processes within thunderstorms, where collisions between different hydrometeors such as graupel, hail, and ice crystals leads to the separation and buildup of electric charges. Therefore, selection and tuning of parameterization schemes, particularly for Microphysics (MP), Cumulus (Cu), and Lightning (LP) processes, play a critical role in enhancing model performance and predictive accuracy.

This study evaluates the performance of the Weather Research and Forecasting (WRF) in simulating lightning for a severe thunderstorm event on May 14, 2022, over Eastern India (West Bengal and Jharkhand). The Indian Lightning Location Network (ILLN) recorded a peak 30-minute flash count ~8000 flashes. A total of 57 combinations of MP-Cu-LP schemes were tested using a three nested domain (27 km, 9 km, and 3 km grid spacing) and analysed the output of the innermost domain (3 km).

Results shows that the LP2 scheme (based on 20 dBZ reflectivity) significantly outperformed LP1 (updraft-based), particularly when combined with the Kain-Fritsch (KF) cumulus scheme enabled in the inner domain. Among MP options, Goddard, Morrison, and WDM-6 schemes produced the best results. The overall best-performing scheme combinations: LP2-KFon-Goddard, LP2-KFon-Morrison, LP2-KFon-WDM5, and LP2-KFoff-WDM6 achieved high correlations (0.91–0.94) with observed lightning flash counts.

Vertical profile analyses revealed that the thermodynamic properties were consistently simulated across parameterization schemes, but microphysical differences influenced the lightning prediction accuracy. The best-performing combination (LP2 – KF_{on} – MP 7 – Goddard) provided balanced cloud water and ice-phase dynamics, while the worst-performing scheme (LP1–KFoff–Morrison) overestimated cloud water and ice content, leading to inaccurate lightning predictions. Therefore, the differences in model performance were not due to representation of large-scale thermodynamic or moisture transport processes but rather stem from representation of microphysical processes, particularly cloud water retention, precipitation efficiency, and ice-phase dynamics. Enhancing the representation of riming efficiency and hydrometeor phase transitions could enhance model accuracy in future lightning prediction

1. INTRODUCTION:

Lightning is a natural electrical phenomenon that occurs when there is a rapid release of accumulated electrical energy between regions of differing electrical charges, either within the atmosphere or between the atmosphere and the ground. This discharge happens when the difference in charge becomes large enough to overcome the resistance of the air, allowing electricity to flow freely. The result is a flash of light, known as a lightning bolt, accompanied by the sound of thunder caused by the rapid expansion and contraction of air due to the intense heat generated by the lightning.

Lightning prediction is crucial for several reasons: (i) It poses a severe threat to human life (ii) spark wildfires (iii) Its strike leads to failure of electrical equipment's (iv) severe impact to aviation industry (v) It's a precursor for severe weather events such as Thunderstorms, Tornadoes and hailstorms.

Operational meteorologists rely on real time data and radar data for lightning information. Numerical weather models do not explicitly simulate lightning. Therefore, we need to parameterise to forecast lightning. Forecasting lightning strikes is impossible because of its frequent and random nature during a thunderstorm. Therefore, meteorologists and forecasters can predict the likelihood of lighting and thunderstorm activity.

Selection and tuning of different parameterization schemes play a pivotal role in combined improvement in the model's performance and its accuracy (Biswasharma et al, 2024)

1.1 Origin of Thunderstorms

The atmosphere is largely transparent to short-wave solar radiation. A part of the incoming radiation is absorbed by the atmosphere, causing it to warm up. This heating process generates atmospheric instability, leading to the ascent of buoyant air parcels to higher altitudes, which plays a crucial role in thunderstorm development. Various mechanisms, such as boundary layer thermals, warm and cold fronts, and orographic lifting, can initiate this vertical movement.

As the air rises, it cools adiabatically at an approximate rate of 10°C per kilometer. Once it cools below its dew point, water vapor condenses around condensation nuclei at slight supersaturation levels. The latent heat released during condensation enhances the buoyancy of the air, keeping the temperature of rising clouds higher than that of their surroundings. As the cloud extends to the freezing level, some droplets freeze, releasing additional latent heat. This further increases the buoyancy, accelerating the upward motion of cloud parcels. In this way, the cloud functions as a massive heat engine, with energy derived from the heat released by condensation and freezing, fuelling the vertical air movement.

1.2 Development of Thunderstorms:

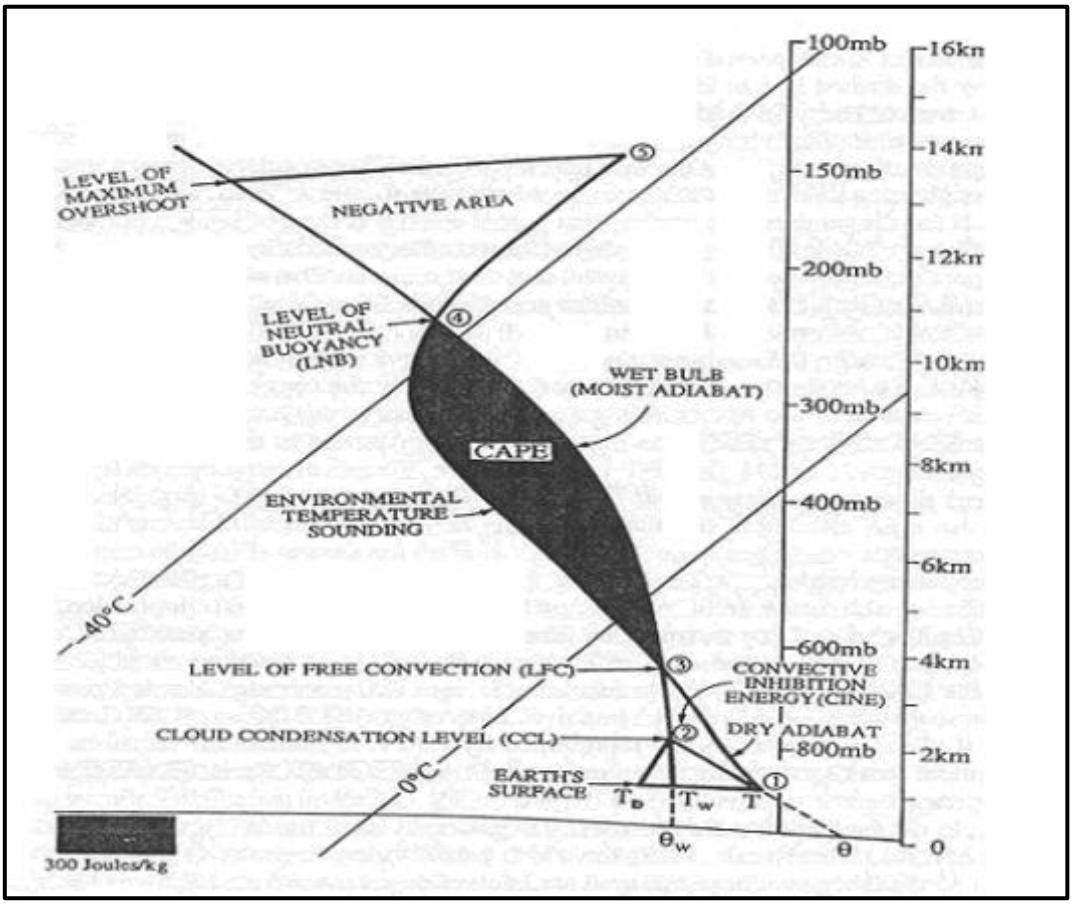

Figure 1: A thermodynamic diagram illustrating the components contributing to conditional instability (from William, 1995)

When an unsaturated air parcel is lifted by external forces such as orographic lifting, convergence lifting, or frontal lifting, it cools at the rate of 10°C / km which is called as Dry Adiabatic Lapse Rate (DALR). When the rising air parcel reaches the Cloud Condensation Level (CCL), it becomes saturated. Beyond this point, water vapor begins to condense, releasing latent heat. This reduces the cooling rate to around 6°C / km, known as the Moist Adiabatic Lapse Rate (MALR).

The Level of Free Convection (LFC) refers to the altitude at which an air parcel's temperature becomes equal to the environmental temperature. From this point onward, the air parcel continues to rise due to its own buoyancy, powered by the heat released during condensation.

The buoyant force experienced by the air parcel is directly proportional to the difference between its virtual temperature and the virtual temperature of the surrounding environment. As a result, the parcel continues ascending until it reaches the Level of Neutral Buoyancy (LNB).

The work done to lift a unit mass of the air parcel through a small height (dz) in the atmosphere is represented as:

$$W = \frac{g\left(T_p - T_e\right) dz}{T_e}$$

where,

W is the work done,

g is the acceleration due to gravity,

T_p is the virtual temperature of the air parcel and

T_e is virtual temperature of the environment.

The total work done in raising the air parcel from the LFC to the LNB is referred to as the Convective Available Potential Energy (CAPE). However, for CAPE to be released, a small amount of energy known as Convective Inhibition (CIN) must be overcome, representing a region of negative energy that acts as a barrier to convection.

1.3 Cloud Droplet Growth and Rain Formation

The Clausius–Clapeyron Equation and Cloud Droplet Formation

The Clausius–Clapeyron equation describes the equilibrium state of a thermodynamic system containing water vapor, liquid water, and ice. As an ascending air parcel reaches its saturation point, water vapor condenses onto cloud condensation nuclei, forming cloud droplets through a process known as heterogeneous nucleation. These droplets initially grow to a size of approximately 10 μm in radius by continued condensation. However, the rate of growth through condensation alone slows down as the droplets increase in size.

To illustrate, a raindrop with a 1 mm diameter has a volume equivalent to about one million cloud droplets of 10 μm radius. Because condensation alone is insufficient for producing large raindrops, two key mechanisms are proposed for droplet growth to raindrop size:

(a) Collision and Coalescence Process

(b) Bergeron Process

(i) Collision and Coalescence Process

This process typically occurs in warm clouds where temperatures remain above 0°C. In this scenario, droplets of varying sizes fall at different terminal velocities, leading to collisions and subsequent coalescence. Larger droplets, having greater velocities, collide with smaller ones, forming even larger drops. When droplets grow too large, aerodynamic forces can overcome surface tension, causing the drops to break into smaller fragments, which may then participate in further collisions. In regions such as the tropics, where water vapor content is high, cloud condensation levels are low, and freezing levels are elevated, this process can result in intense rainfall. Although primarily responsible for rain formation in warm clouds, the collision and coalescence process can also contribute to the development of rain, graupel, or hail in cloud areas below freezing, where supercooled water exists. Lightning has occasionally been observed in these warm clouds, although conflicting studies suggest that ice-phase processes are generally essential for thunderstorm electrification.

(ii) Bergeron Process

In colder clouds, where temperatures drop below 0°C, an air parcel may experience a mixed-phase environment, consisting of vapor, liquid water, and ice. Because ice has a lower equilibrium vapor pressure than liquid water at the same temperature, water vapor tends to deposit onto ice crystals. To maintain balance, nearby water droplets evaporate, providing more vapor for the ice crystals to grow. This process is driven by the Clausius–Clapeyron relationship.

As ice crystals continue to grow through vapor deposition, they may reach sizes where their terminal velocities become significant. Subsequently, they begin to collect supercooled water droplets in a process known as accretion or riming. The supercooled droplets freeze instantly upon contact with the ice, forming graupel — porous ice particles with a lower density than solid ice.

Depending on the liquid water content within the cloud, ice growth may follow different patterns. Under low liquid water content, ice particles primarily grow by vapor deposition, referred to as dry growth.

Conversely, when the liquid water content is high, the riming process dominates, and the latent heat released during freezing maintains a wet surface on the ice particle. This is known as wet growth. In typical thunderstorms, which have moderate liquid water content, ice particles often undergo dry growth while simultaneously losing mass due to sublimation.

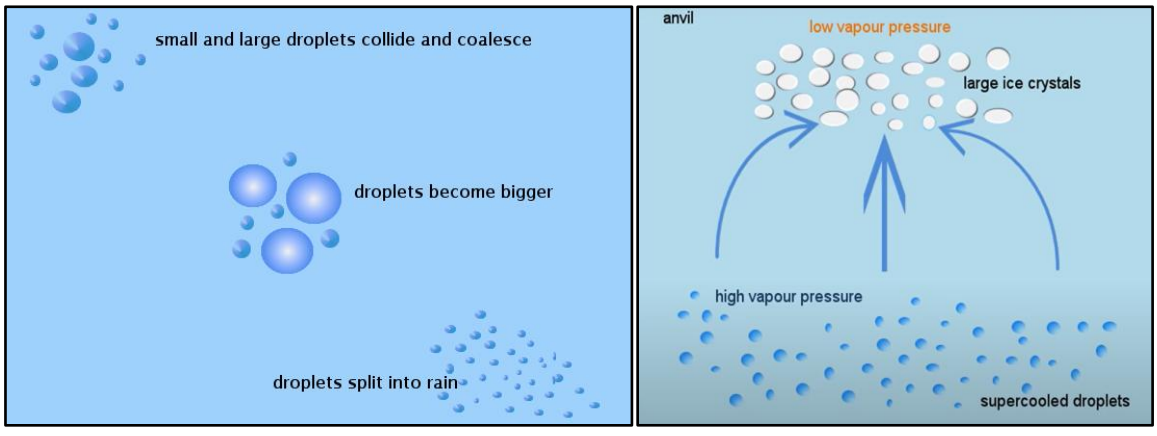

Figure 2: (a) Image depicting the Collision and Coalescence Process and (b) Image depicting the Bergeron Process

1.4 Parameterisation for Cloud Microphysics

In atmospheric modelling, cloud and precipitation processes are represented using microphysics schemes. Two primary approaches exist for parameterizing these processes: bulk microphysics schemes (BMPs) and bin microphysics schemes (BMSs).

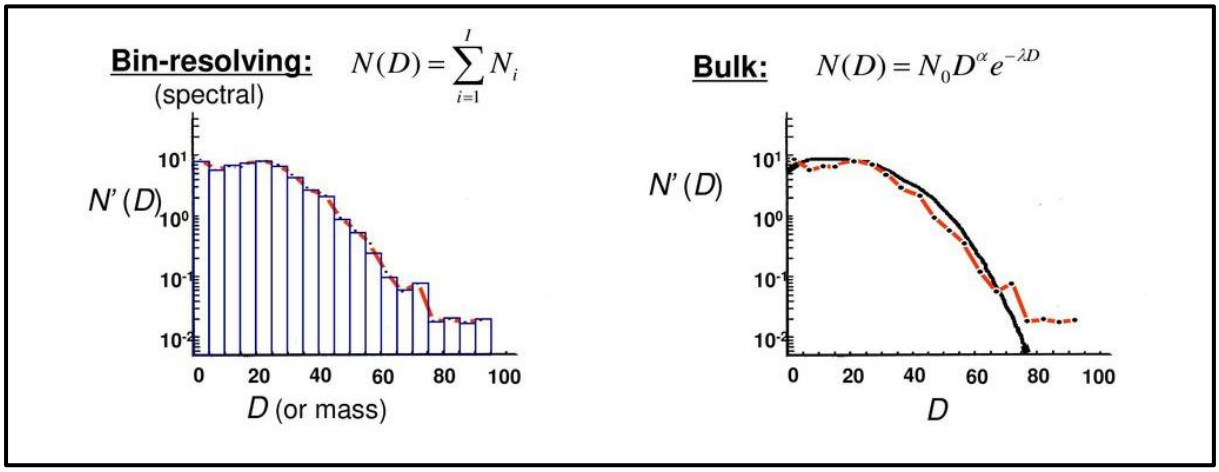

Figure 3: Image explaining the bin and bulk microphysics

(i) Bulk Microphysics Scheme:

Bulk microphysics schemes are commonly employed in numerical weather prediction (NWP) models due to their computational efficiency. They represent the size distribution of cloud particles using simplified mathematical functions, often assuming gamma or exponential distributions. Single-moment bulk schemes predict only the mixing ratio of hydrometeors, whereas double-moment schemes estimate both the number concentration and mixing ratio of hydrometeors.

These schemes integrate over the assumed particle size distribution to approximate the effects of microphysical processes such as condensation, evaporation, deposition, and riming. While bulk schemes are computationally efficient, their accuracy is often limited by the constraints of the assumed size distributions and the simplified parameterizations. Examples of widely used bulk microphysics schemes include the Morrison double-moment scheme, the Thompson scheme, and the WSM6 scheme

(ii) Bin Microphysics Scheme:

Bin microphysics schemes, on the other hand, offer a more detailed and physically accurate representation of cloud microphysics. They explicitly resolve the particle size distribution by dividing it into discrete size bins, typically ranging from a few tens to hundreds of categories. Each bin tracks the number concentration and mass of particles within a specific size range. This allows for a more realistic simulation of microphysical processes, including the growth, collision, and breakup of cloud droplets and ice particles. BMSs are particularly useful for understanding the detailed evolution of hydrometeors and investigating cloud-aerosol interactions. However, their high computational cost makes them less practical for operational forecasting. Examples of bin microphysics schemes include the Hebrew University Cloud Model (HUCM) and the National Severe Storms Laboratory (NSSL) bin scheme.

Choice of Microphysics schemes:

Numerous studies have demonstrated that BMSs often provide more accurate simulations of precipitation intensity and cloud dynamics compared to BMPs. For example, in cases of deep convective clouds, bin schemes generally exhibit stronger updrafts and higher latent heat release due to their more accurate depiction of microphysical processes. Conversely, bulk schemes may underestimate precipitation intensity and misrepresent hydrometeor distributions.

Nevertheless, the choice between bulk and bin schemes depends on the application. Operational models prioritize computational speed, making bulk schemes preferable, whereas research-oriented studies often employ bin schemes for detailed microphysical analysis. Additionally, hybrid approaches and ongoing advancements in BMPs aim to bridge the accuracy gap by incorporating elements of bin scheme physics into bulk parameterizations.

In summary, while bulk microphysics schemes remain the standard for operational weather forecasting due to their efficiency, bin microphysics schemes offer unparalleled accuracy for studying cloud microphysical processes. Understanding the strengths and limitations of each approach is essential for selecting the appropriate scheme for specific meteorological applications.

1.5 Charge Distribution in the Thunderclouds

1.5.1 Electrical Structure of the Thundercloud

Despite extensive research, the exact mechanism behind thunderstorm electrification remains unresolved due to the complex and short-lived nature of thunderstorms. The thunderstorm's electrification process is influenced by several factors such as temperature, humidity, atmospheric stability, ice-water content, and aerosols.

Early theories proposed by Wilson (1920) and Simpson (1927) described the charge distribution in thunderstorms as positive and negative dipoles. The positive dipole structure is when the cloud top has positive charges and the cloud base has negative charges and vice-versa for negative dipole. However, subsequent observations identified a more intricate tripole structure, consisting of a positive charge region at the top, a larger negative region below it, and a smaller positive region near the cloud base.

While remote measurements using electric fields offer a general understanding of thunderstorm charge distribution, balloon soundings have shown that the actual structure can be even more complex, often revealing multiple charge regions. Furthermore, lightning itself can significantly alter the distribution of charges within a storm.

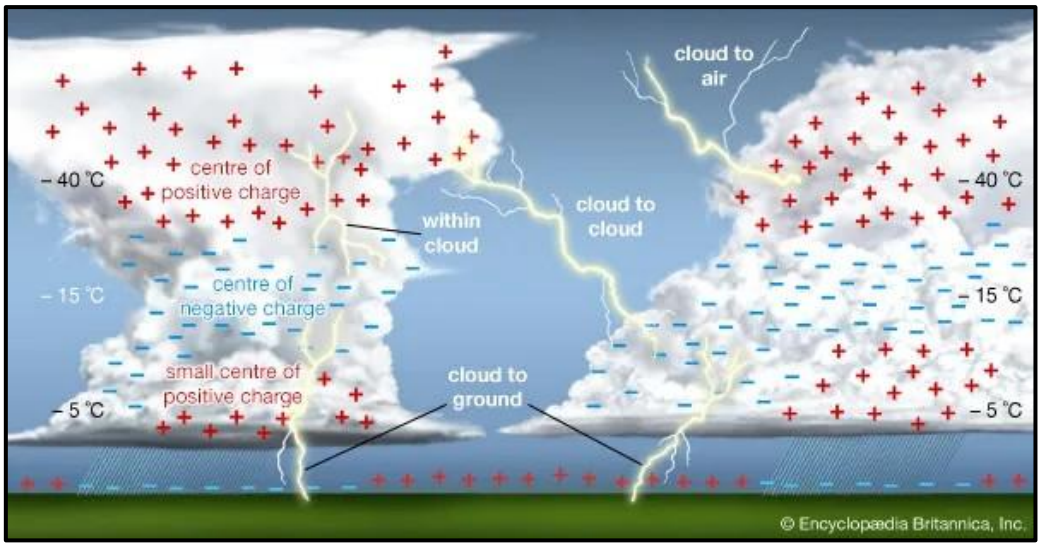

Figure 4: Illustration of the electrical charge distribution within the thundercloud (Krider, E.P. 2025)

1.5.2 Different Charge region within the Thundercloud

The primary negative charge is typically found at altitudes with temperatures between 0°C and -25°C (Simpson and Scrase, 1937; Reynolds and Neill, 1955). Observations show a strong correlation between updraft intensity and charge region elevation (Stolzenburg et al., 1998). Few studies have reported the existence of inverted polarity in thunderclouds (Montanya et al., 2007).

Lower Positive Charge Centres (LPCC), first identified by Simpson and Scrase (1937), are confirmed through numerous studies (Simpson and Robinson, 1941). They are often small, localized, and transient, typically consisting of positively charged precipitation. Some observations suggest they result from lightning-induced charge deposition.

1.5.3 Charges in the Screening Layer

Upper positive charges attract negative ions from the surrounding atmosphere, forming screening layers near the cloud's boundary. These thin layers (Brown et al., 1971) can partially shield the internal charge within seconds. Observations indicate that while screening layers form, they do not always fully develop (Gish and Wait, 1950). Some theories propose that the negative charge in the screening layer descends to contribute to the main negative charge region (Vonnegut, 1953; Krehbiel, 1986)

1.6 Thunderstorm Electrification – Charging Mechanisms

(i) Convective Charging:

The convective charging mechanism suggests that as a cumulus cloud grows, it draws positive charges from cloud base, which are carried upwards by the updraft. Few negative ions from the surrounding atmosphere are accumulated near the cloud top forming a negative screening layer. The negative charge within the screening layer moves downward as the layer descends, gathering in the lower regions of the cloud. This accumulation intensifies the separation of charges between the cloud and the ground, leading to a strengthening of the surface electric field.

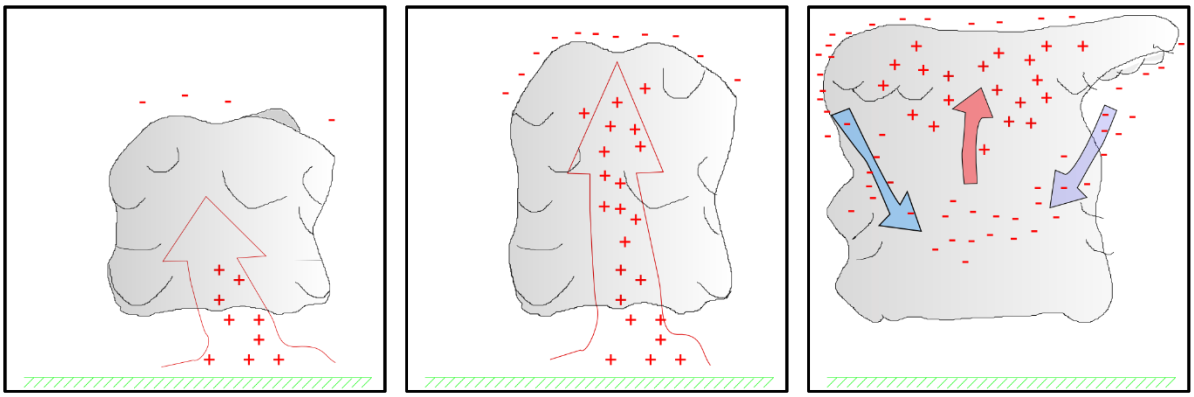

Figure 5 (a): Illustration depicting the convective charging mechanism

When the field becomes strong enough, it can trigger corona discharges at the Earth's surface, generating more positive ions that reinforce the process. While early estimates suggested this mechanism could explain the electrical energy in clouds, later observations raised doubts, as there was limited evidence of positive charge transport from the ground to the cloud. However, some events, like increased lightning following the Chernobyl accident, imply that atmospheric ions could still influence cloud electrification.

(ii) Inductive Charging

The inductive charging mechanism refers to the process where the cloud particles get polarised due to the presence of vertical electric field within the thundercloud. When larger particles, like graupel, fall and collide with smaller particles, like ice crystals or droplets, charge is transferred — smaller particles usually gain a positive charge, while larger particles become negatively charged. The different fall speeds of these particles lead to a separation of charges, forming a dipole with positive charge higher up and negative charge below. However, this mechanism alone is unlikely to generate the strong electric fields needed for lightning, as factors like short contact times and opposing electrical forces can limit its effectiveness. While it may not be sufficient as the primary driver of thunderstorm electrification, it can contribute to the complex charge structures observed in storms, especially after other mechanisms have initiated the charge buildup.

(a) Selective ion capture:

The Earth's electric field causes charge separation within individual cloud particles, resulting in a negative charge at the top and a positive charge at the bottom. As these particles descend through the cloud, they attract free negative ions to their lower surfaces. However, positive ions are unable to catch up and attach to the upper surfaces. This process leads to a net negative charge accumulating in the lower, warmer part of the cloud, while the upper, colder region is left with a net positive charge. Although this theory explains the observed polarity, it is only effective under weak electric fields and is therefore not quantitatively reliable.

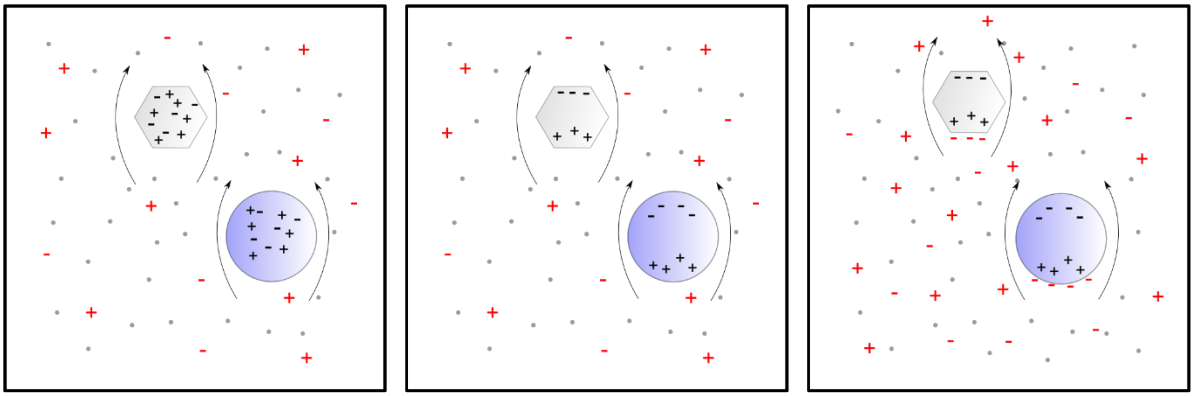

Figure 5 (b): Illustration depicting Selective ion capture (Inductive charging)

(b) Rebound of particles:

Charge separation within individual cloud particles can occur due to the Earth's electric field, resulting in a negative charge at the top and a positive charge at the bottom. When a larger, faster-falling particle collides with a smaller one, the larger particle, having a greater surface area, tends to gain a net negative charge, while the smaller particle acquires a net positive charge. The heavier, negatively charged particle then descends to the lower, warmer region of the cloud, while the lighter, positively charged particle is carried upward.

A significant issue with this theory is its reliance on the assumption that collisions occur in a way that aligns the positive and negative surface regions of the colliding particles, which is not always guaranteed.

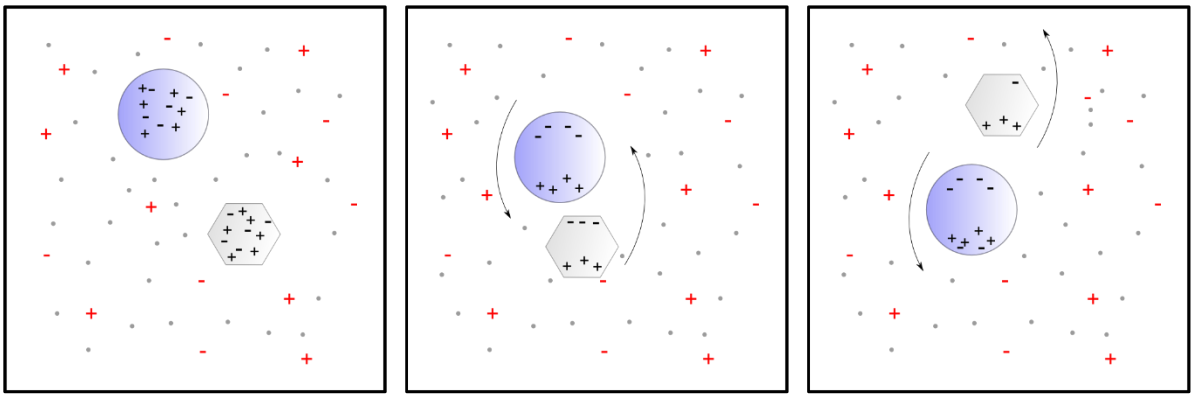

Figure 5 (c): Illustration depicting Rebound of particles (Inductive charging)

(iii) Non-Inductive Charging

Non-inductive charging refers to the process of charge transfer between particles during collisions, without relying on the local electric field. In thunderstorms, when ice crystals collide with riming graupel (ice-covered particles), they gain opposite charges. This charge separation, driven by gravity, leads to the formation of the characteristic vertical dipole structure in clouds. Initially, researchers believed temperature differences caused this effect, but later studies showed that factors like liquid water content and cloud temperature are more influential. The charge transfer can even reverse depending on these conditions, with faster-growing particles tending to acquire a positive charge. While this mechanism explains many observations of thunderstorm electrification, the presence of strong lower positive charge centers and complex charge structures in some storms suggests that other mechanisms may also play a role.

a. Thermoelectric effect:

When a hailstone collides with a colder ice crystal, the temperature gradient at the contact point causes a charge transfer. Since H+ ions move faster than OH- ions in the ice lattice, the colder particle gains a net positive charge. However, the conditions required for this effect, like high impact velocities and large temperature differences, are unlikely in clouds.

b. Riming Electrification:

When graupel collides with ice crystals in a cloud containing super-cooled water vapor, significant charge transfer can occur. The magnitude and sign of the charge depend on the temperature and cloud water content (CWC). At temperatures below -20°C, graupel typically gains a negative charge and descends, while positively charged ice crystals remain at higher altitudes. In warmer mid-level regions, graupel tends to acquire a positive charge, with negatively charged ice crystals lingering at mid-levels, contributing to the cloud's overall negative charge. This process helps explain the tripole charge structure seen in many clouds.

However, in clouds with high moisture content, such as oceanic clouds, charge transfer is reduced, leading to fewer lightning strikes. While riming electrification is considered a primary charging mechanism, the exact reason why graupel and ice crystal collisions produce specific charge behaviours remains unclear.

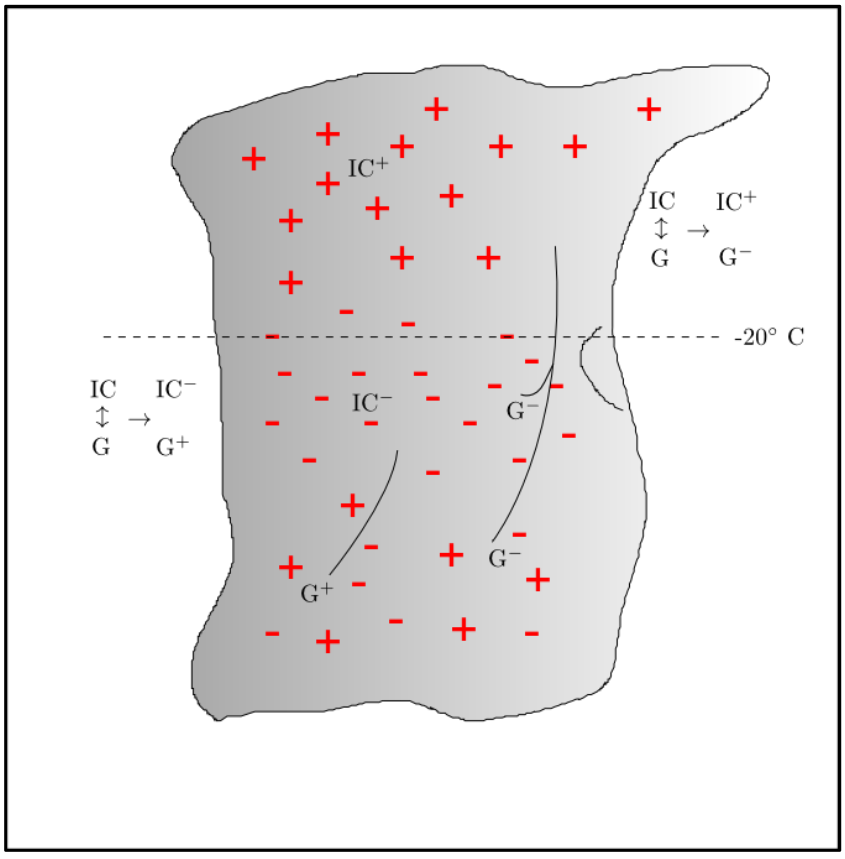

Figure 5 (d): Illustration depicting the Riming electrification process

1.7 Parameterisation for Lightning Prediction

Lightning parameterization schemes are used in weather and climate models to estimate lightning activity based on storm characteristics. These schemes avoid the complexity and computational cost of simulating electrical processes directly, therefore use observable storm parameters as proxies for lightning prediction.

Price and Rind (1992) developed a widely referenced lightning parameterization that relates lightning flash rates to cloud top height (CTH) and maximum vertical velocity (w_{max}). Their research built on earlier findings that indicated a strong positive correlation between the extent of a storm's vertical development and its lightning activity. This relationship is particularly useful in global and regional models where direct simulation of lightning is impractical.

a) LP1 Scheme: Based on maximum vertical updrafts (w_{max}):

$$f = 5 \times 10^{-6} \times (w_{max})^{4.5}$$

w_{max} is the strongest upward air motion within the storm, often observed in convective updrafts. Vertical velocities are closely linked to the storm's severity and electrification potential. This approach is particularly useful in distinguishing between maritime and continental convection, as continental storms tend to have stronger updrafts and produce more lightning.

b) LP2 Scheme: Based on Convective cloud top height (CTH):

$$f = 3.44 \times 10^{-5} \times CTH^{4.9}$$

CTH refers to the maximum height of the cloud where the radar reflectivity exceeds 20 dBZ and temperatures are below freezing (0°C). The empirical relationship developed by Price and Rind associates taller clouds with increased lightning frequency, recognizing that stronger updrafts and larger ice crystal formations contribute to enhanced charge separation and lightning generation. This non-linear relationship reflects the rapid increase in lightning activity with taller clouds.

2. DATASETS, MODEL CONFIGURATION AND METHODS:

2.1 DATASETS:

2.1.1 India Lightning Location Network (ILLN) Sensor Data:

The analysis in this study uses data from the Indian Lightning Location Network (ILLN) sensors. ILLN data is preferred due to its advantages, including (i) the reliability of ground-based observations, (ii) high spatial and temporal resolution, and (iii) a 90% accuracy rate in detecting lightning.

The ILLN currently operates 83 sensors distributed across India (Figure 6). These sensors capture lightning flash rate per second, geographic coordinates (latitude and longitude), and lightning type, distinguishing between intra-cloud (IC) and cloud-to-ground (CG) discharges. The detection efficiency is 90% for CG flashes and 50% for IC flashes.

Lightning flashes are detected using frequencies ranging from 1 Hz to 12 MHz. Lower frequencies (1 Hz to 1 kHz) are primarily used for CG discharge detection, while intermediate frequencies (1 kHz to 1 MHz) capture return strokes. Higher frequencies (1 MHz to 12 MHz) are effective in identifying intra-cloud and inter-cloud flashes (Biswasharma, et al., 2024).

During a lightning event, electromagnetic energy is radiated outward in all directions (Pawar et al., 2023). Each sensor records the full waveform of the event and transmits compressed data to the central detection server. The complete waveform data, rather than just the peak amplitude, is valuable for distinguishing between CG and IC flashes.

The lightning flash mapping process relies on the Time of Arrival (TOA) technique. This method uses the arrival times of electromagnetic signals at multiple sensors to accurately determine the lightning stroke location. By correlating waveforms and calculating arrival times, the peak current and precise location (latitude, longitude, and altitude) are determined.

A lightning flash is identified when strokes occur within 700 milliseconds and within a 10 km radius of the initial detected stroke. If a flash contains at least one return stroke (Mohan et al., 2021), it is classified as a CG flash; otherwise, it is categorized as an IC flash.

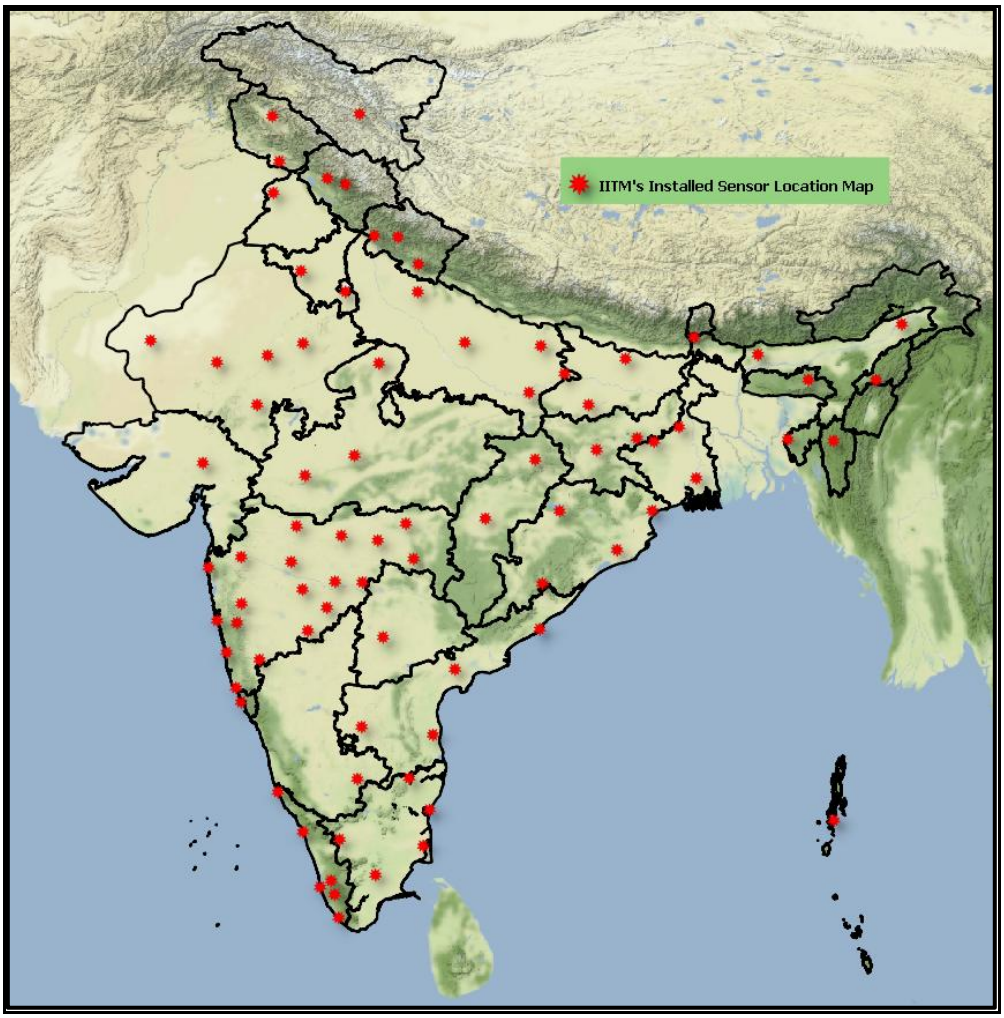

Figure 6: Location of ILLN sensors in different parts of India

2.1.2 NCEP FNL Data:

National Center for Environmental Prediction – Final run (NCEP FNL) data (Biswasharma et al, 2024) is a renowned dataset in the atmospheric community for representing the atmospheric condition. It has a spatial and temporal resolution of 1° × 1° and of six hours respectively.

It includes atmospheric parameters such as Temperature, Relative Humidity, Geopotential height, u- and v- winds, vertical motion, surface pressure, etc.

2.2 WRF MODEL:

This study utilized the Advanced Research Weather Research and Forecasting (WRF-ARW model version 4.5), to simulate thunderstorm events. The WRF model is a fully compressible, non-hydrostatic mesoscale model having two Eulerian mass dynamical cores.

The WRF model has various physics: Microphysics (MP) schemes, Cumulus (Cu) schemes, Radiation schemes, PBL schemes, Land surface and surface layer schemes and Lightning parameterisation schemes.

In this study, we have used Three nested domain with 27 km × 27 km, 9 km × 9 km and 3 km × 3km as their horizontal resolution (Figure 7) and the output of the innermost domain was studied. The initial and boundary condition for the WRF model run is obtained from the NCEP FNL data.

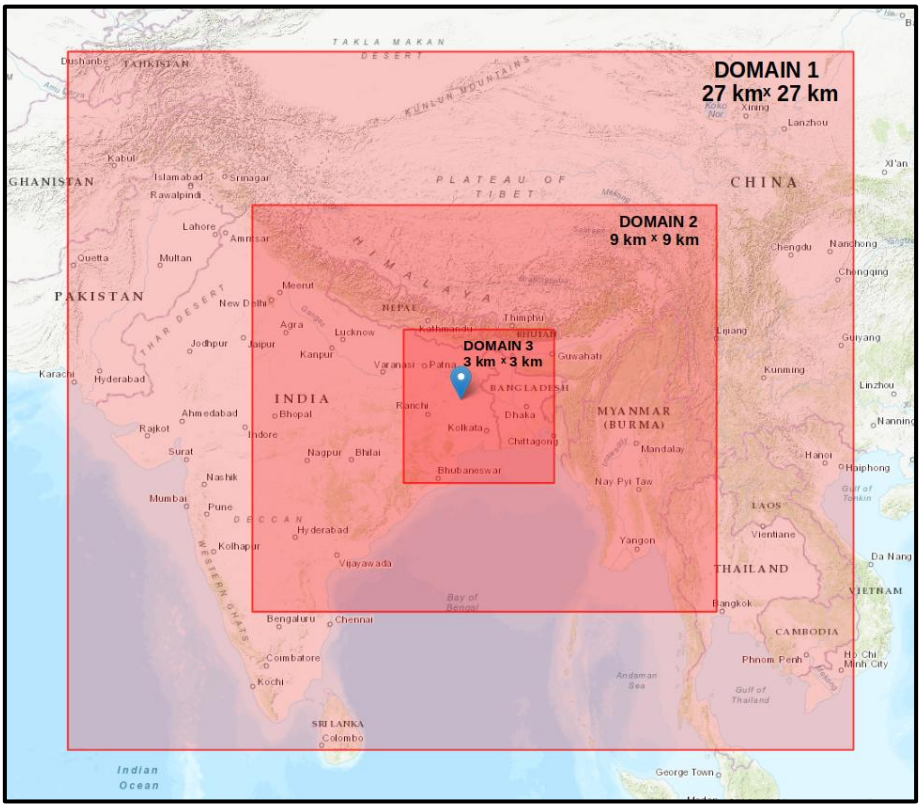

Figure 7: Three nested domains used in the WRF model

A total of 56 combinations of various microphysics, cumulus and lightning parameterisation schemes were studied. Seven Microphysics schemes, Two Cumulus schemes, and two Lightning Parameterisation schemes were assessed. Refer Table 1 and Table 2 for the details about the model configuration and concise description of various schemes.

CASE STUDY	
Thunderstorm Case study	May 14, 2022 – West Bengal
Simulation Period	30 Hours (May 13, 2022 18 UTC – May 15, 2022 00 UTC)
MODEL CONFIGURATION:	
Model	WRF Model Version 4.5 – ARW core
Dynamics	Non – Hydrostatic
Map projection	Mercator
IC/BC condition	NCEP FNL with resolution 1° x 1°
Domain configuration	Spatial resolution: 27x27, 9x9, 3x3 (in km) Time resolution: 30 minutes Vertical levels: 45
PARAMETERISATION SCHEMES:	
Microphysics	M6, M7, M8, M9, M10, M14, M16
Cumulus	KF, MSK
Planetary Boundary layer	YSU
Surface layer physics	Revised MM5
Shortwave radiation	Dudhia
Longwave radiation	RRTM
Lightning Options	L1, L2, L3
IC CG method	1, 2, 3

Table 1: The WRF model Configuration

MP Option	Scheme	Mass variables	Number variables	Details
M6	WSM6	Qc Qr Qi Qs Qg	N/A	Hong and Lim (2006)
M7	Goddard 4-ice	Qc Qr Qi Qs Qg Qh	N/A	Tao et al (1989, 2016)
M8	Thompson	Qc Qr Qi Qs Qg	Ni Nr	Thompson et al., (2008)
M9	Milbrandt 2-mom	Qc Qr Qi Qs Qg Qh	Nc Nr Ni Ns Ng Nh	Milbrandt and Yao (2005)
M10	Morrison 2-mom	Qc Qr Qi Qs Qg	Nr Ni Ns Ng	Morrison et al., (2009)
M14	WDM5	Qc Qr Qi Qs	Nn Nc Nr	Lim and Hong (2010)
M16	WDM6	Qc Qr Qi Qs Qg	Nn Nc Nr	Lim and Hong (2010)

Table 2 (a):

Concise description of various Microphysics (MP) schemes that was used in the study

LP Options	Scheme	Details
L1	PR92 – based on max. w	Price and Rind (1992)
L2	PR92 – based on 20 dbz top	Price and Rind (1992)

Table 2 (b):

Concise description of various Lightning (LP) schemes that was used in the study

Cu Option	Scheme	Moisture Tendencies	Details
KF	Kain-Fritsch	Cloud, rain, ice, snow	Kain and Fritsch (1993)
MSK	Multiscale Kain-Fritsch	Cloud, rain, ice, snow	Kain (2004)

Table 2 (c):

Concise description of various Cumulus (Cu) schemes that was used in the study

2.3 METHODOLOGY:

2.3.1 Gridding of ILLN sensor Data

The ILLN sensor data has a spatial accuracy of 300 m and temporal resolution of nanoseconds. To compare the ILLN sensor data with the WRF outputs, the data has been gridded in 3 km × 3 km bins and 30-minute hourly time steps. Lightning data outside the Indian continental region has been removed. The Time has been converted from UTC to IST.

2.3.2 Different combination of the Model runs:

Two Lightning Parameterisation (LP): (Price and Rind 1992)

a) **LP1**: Based on maximum vertical updrafts (w_{max})
b) **LP2**: Based on Convective cloud top heigh (CTH)

Two Cumulus Parameterisation (Cu):

a) **Kain-Fritsch (KF)** – turned on/off for the innermost domain
b) **Multiscale Kain-Fritsch (MSK)** - turned on/off for the innermost domain

Seven Microphysics Parameterisation (MP):

MP 6: WSM-6
MP 7: Goddard 4-ice
MP 8: Thompson
MP 9: Milbrandt 2-mom
MP 10: Morrison 2-mom
MP 14: WDM-5
MP 16: WDM-6

	KF_{on}	KF_{off}	MSK_{on}	MSK_{off}
LP 1	For 7 MP schemes	For 7 MP schemes	For 7 MP schemes	For 7 MP schemes
LP 2	For 7 MP schemes	For 7 MP schemes	For 7 MP schemes	For 7 MP schemes

Table 3: Table representing 56 Various Combinations of parameterisation schemes used in the study. Each of the LP and CU Schemes were simulated for seven different MP schemes giving 56 LP – CU - MP combinations which were analysed in the study.

2.3.3 Model sensitivity Analysis:

The forecasted output of the WRF model for each parameterisation combination is compared with the Observational data (ILLN Lightning sensor data). Correlation co-efficient (CC), Standard deviation (STD) and Root Mean Square Difference ($RMSD$) are computed for various combinations of MP, CU, LP schemes (Biswasharma et al, 2024)

1. The **Correlation Coefficient** ($\boldsymbol{CC}$) is a statistical measure to identify the correlation between two variables. The correlation co-efficient is calculated using the formula:

$$CC = \frac{\sum_{i=1}^{N}(o_i - \bar{o})(m_i - \bar{m})}{\left(\sqrt{\frac{1}{N}\sum_{i=1}^{N}(o_i - \bar{o})^2}\right)\left(\sqrt{\frac{1}{N}\sum_{i=1}^{N}(m_i - \bar{m})^2}\right)}$$

2. **Standard deviation ($\boldsymbol{STD}$)** is a statistical measure that describes the dispersion or spread of datas around the mean of the dataset. It is calculated using the formula:

$$STD = \sqrt{\frac{1}{N}\sum_{i=1}^{N}(x_i - \bar{x})^2}$$

where, x_i represent each data value, $\bar{x}$ represents the mean value of the dataset and N represents total number of data points in the dataset.

3. The **Root Mean Square Difference ($\boldsymbol{RMSD}$)** is an accuracy measure to compare forecasting errors associated with different model runs of a particular dataset.

$$RMSD = \sqrt{\frac{1}{N}\sum_{i=1}^{N}(m_i - \bar{o})^2}$$

To plot Taylor diagram using CC, STD and RMSD, RMSD is computed using the formula:

$$RMSD = (\sigma_o^2 + \sigma_m^2 - 2\,\rho\,\sigma_o\sigma_m)$$

where, σ_o is the STD of observed dataset, σ_m is the STD of model output and ρ is the CC between model data and observed data.

3. RESULTS AND DISCUSSIONS:

3.1 Flash count Spatial distribution in India:

I. Yearly Averaged Flash counts (2019 – 2023):

At the outset, the spatial distribution of total flash counts over India during the five-year period is analyzed (Figure 8). The results highlight dominant lightning activity over Eastern India, particularly covering West Bengal, Bihar, Odisha, and eastern Madhya Pradesh. Northeastern India, especially around the Meghalaya Plateau, emerges as another hotspot. Significant lightning activity is also observed along the southwestern coast and the eastern coastal regions and the himalayan foothills.

A detailed systematic discussion on the spatial distribution of lightning during this period is provided in Biswasharma et al. (2025). Given that the highest lightning activity is concentrated over Eastern India, we selected the West Bengal region for simulating the thunderstorm.

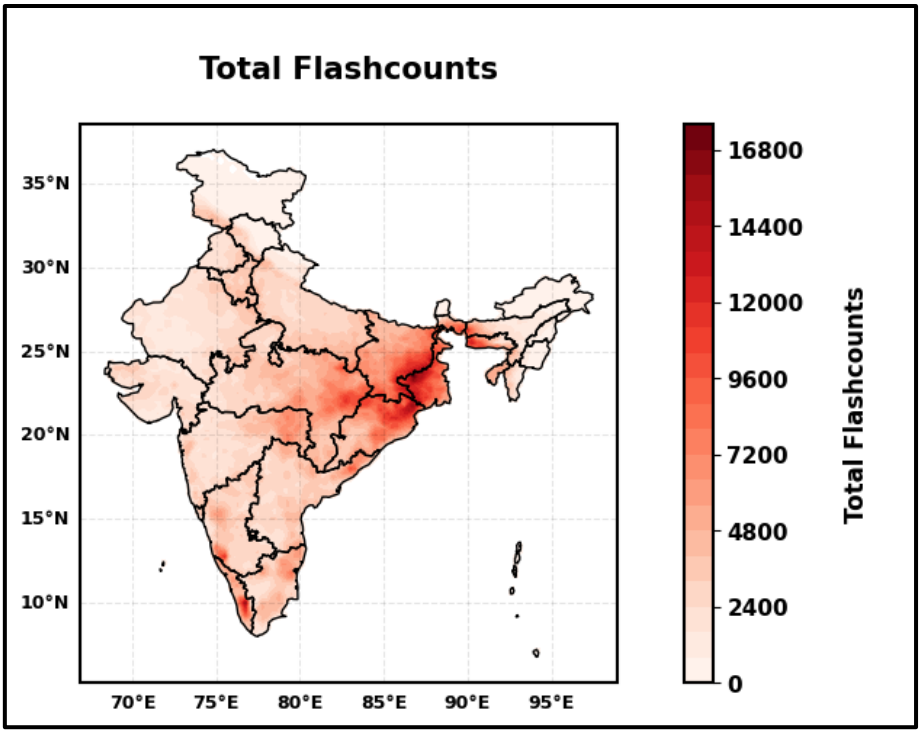

Figure 8: Yearly averaged spatial distribution of flash counts in India

II. Seasonal distribution of Flash counts:

The seasonal distribution of lightning over India is presented in Figure 9. As widely recognized, lightning activity is at its minimum during winter, peaks during the monsoon, and is followed by significant activity in the pre-monsoon season (Ranalkar and Chaudhari, 2009). Notably, the transition months of May and June exhibit the highest lightning occurrence across India (not shown here).

During the monsoon, increased lightning activity is also observed over North-western India, particularly in Kashmir and its neighbouring regions. Meanwhile, the western coast sees higher lightning activity during the pre-monsoon, whereas the eastern coast experiences a peak during the post monsoon season.

Eastern India consistently experiences the highest flash density during both pre-monsoon and monsoon seasons. This also emphasize the need for better simulation and prediction of lightning especially over Easten India region.

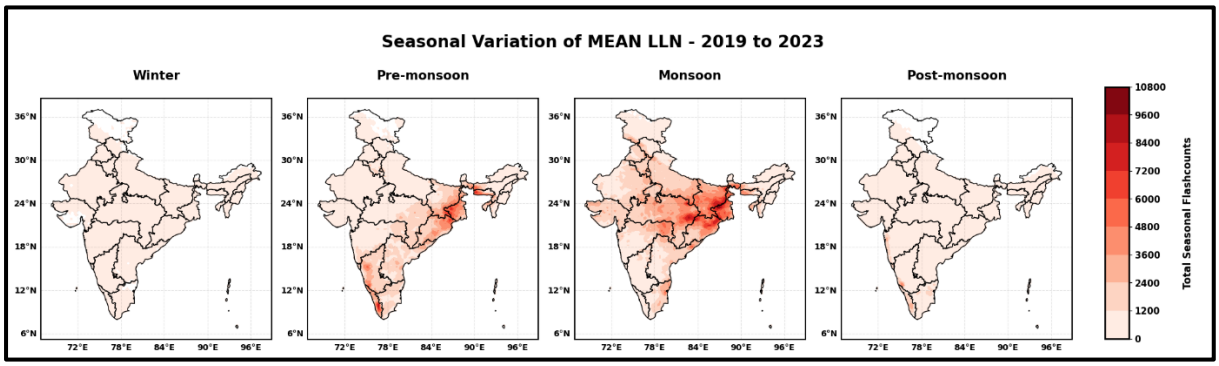

Figure 9: Spatial distribution of flash counts for four different seasons in India

3.2 Overview of the Thunderstorm Event on 14th May 2022:

The thunderstorm activity on May 14, 2022, near East India (covering the borders of West Bengal, Odisha, and Bihar) recorded a peak lightning activity of approximately 8,000 flashes. The afternoon thunderstorm persisted for around five hours. A secondary peak was observed during 00:00 IST - 02:00 IST on May 15.

Figure 10(a) and 10(b) illustrate the diurnal and spatial distribution of lightning flashes associated with the storm.

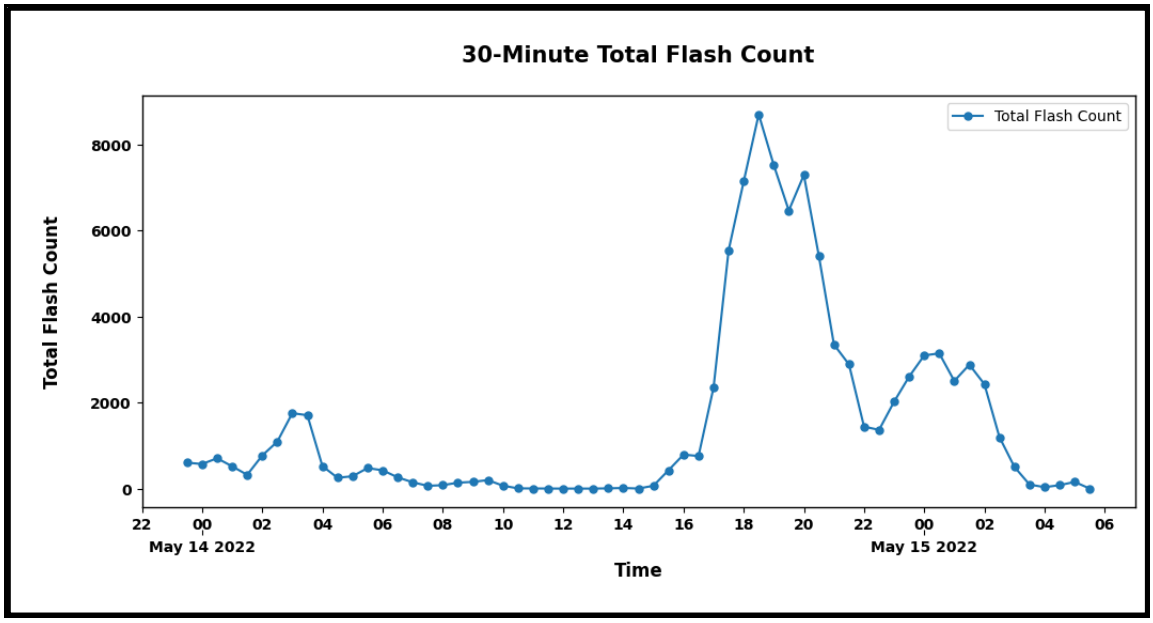

Figure 10 (a): Temporal variation of the 30-minute lightning flash

The spatial distribution indicates that the thunderstorm was initiated around 15:00 IST near the West Bengal-Bihar border and intensified in the following hours. By 21:00 IST, the storm began to dissipate. Overall, the thunderstorm did not exhibit significant movement but showed an increase in areal extent as it evolved.

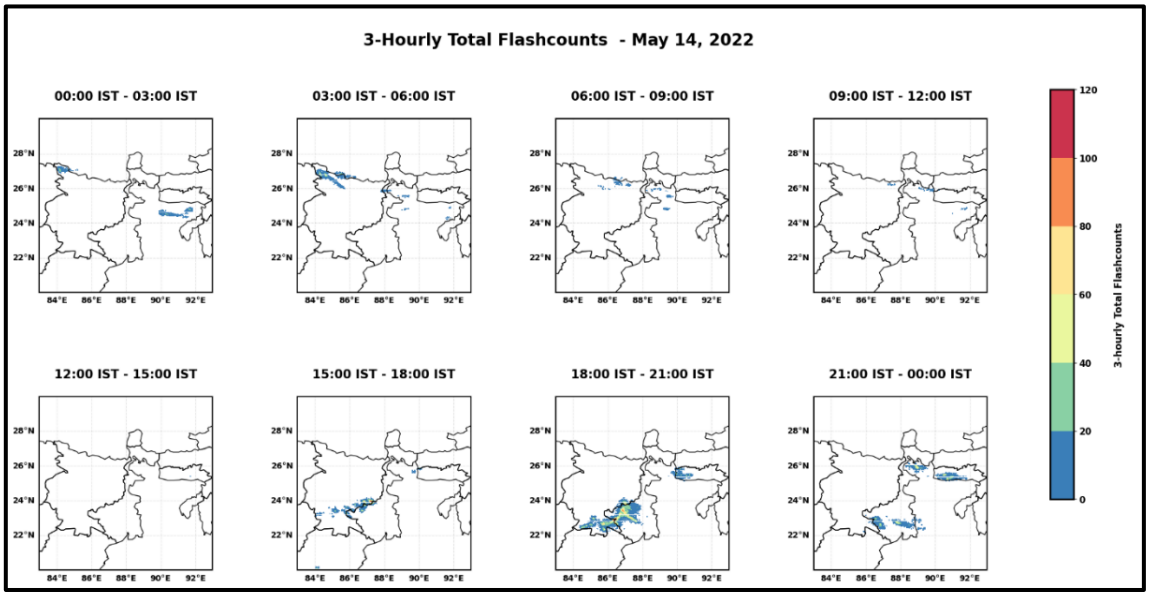

Figure 10 (b): Spatial Distribution of the lightning flashes as observed by ILLN

3.3 Evaluation of Various parameterisation schemes:

3.3.1 Lightning Parameterisation:

Lightning parameterisation (LP) options allows prediction of flash rates without chemistry options.

A. **The intra-cloud (IC) to cloud-to-ground (CG) partitioning method** (referred to as iccg_method) offers three options:

- **iccg_method 1**: Extracts only CG flashes.
- **iccg_method 2**: Uses a coarse climatology (Boccippio et al., n.d.). from the 1995-1999 NLDN/OTD data
- **iccg_method 3**: Based on Price and Rind 1993, determines the partitioning based on cold cloud depth

It is found that iccg_method 1 and 2 cannot predict IC flashes. Only iccg_method 3 can efficiently partition IC and CG flashes than other iccg_methods (Figure: 11(a)). Therefore, iccg_method 3 is used in the model configuration.

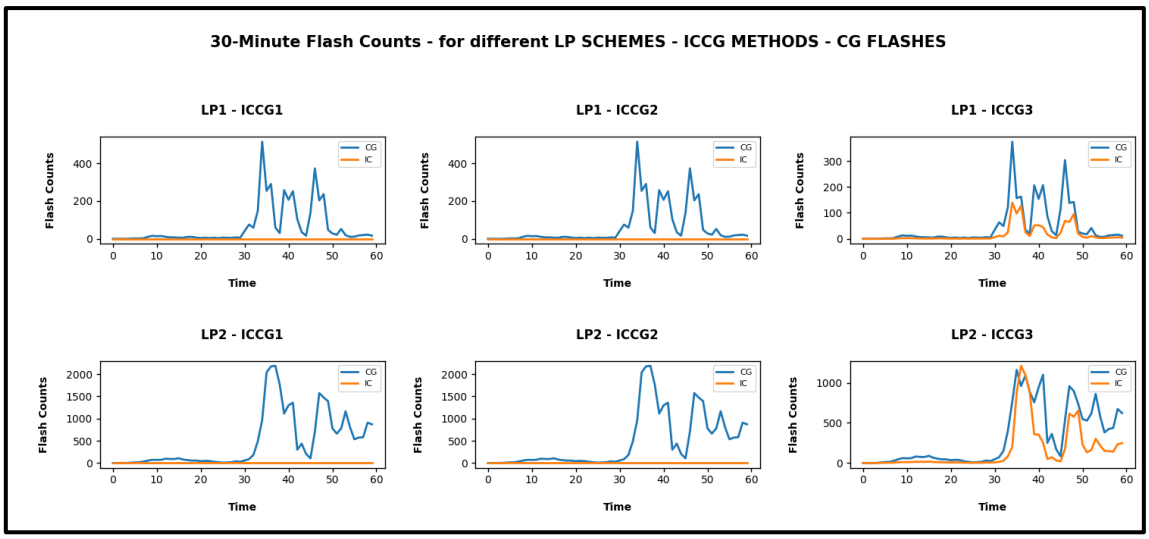

Figure 11 (a): Simulated flash counts for different iccg_methods

B. Price and Rind (1992) Lightning Parameterisation schemes:

Price and Rind (1992) developed a widely used lightning parameterization that relates lightning flash rates to cloud top height (CTH) and maximum vertical velocity (w_{max}). Refer Section 1.7 for more details.

(i) PR92 - LP1 Scheme: Based on maximum vertical updrafts (w_{max}):

$$f = 5 \times 10^{-6} \times (w_{max})^{4.5}$$

(ii) PR92 - LP2 Scheme: Based on Convective cloud top heigh (CTH):

$$f = 3.44 \times 10^{-5} \times CTH^{4.9}$$

Using iccg_method 3, LP1 and LP2 schemes were tested in the WRF model for thunderstorm event. Total flash counts (IC flashes + CG flashes) were calculated and plotted for each scheme (Figure 11(b)). Among the LP schemes, LP2 performs better, whereas LP1 severely underestimates the observed flash counts.

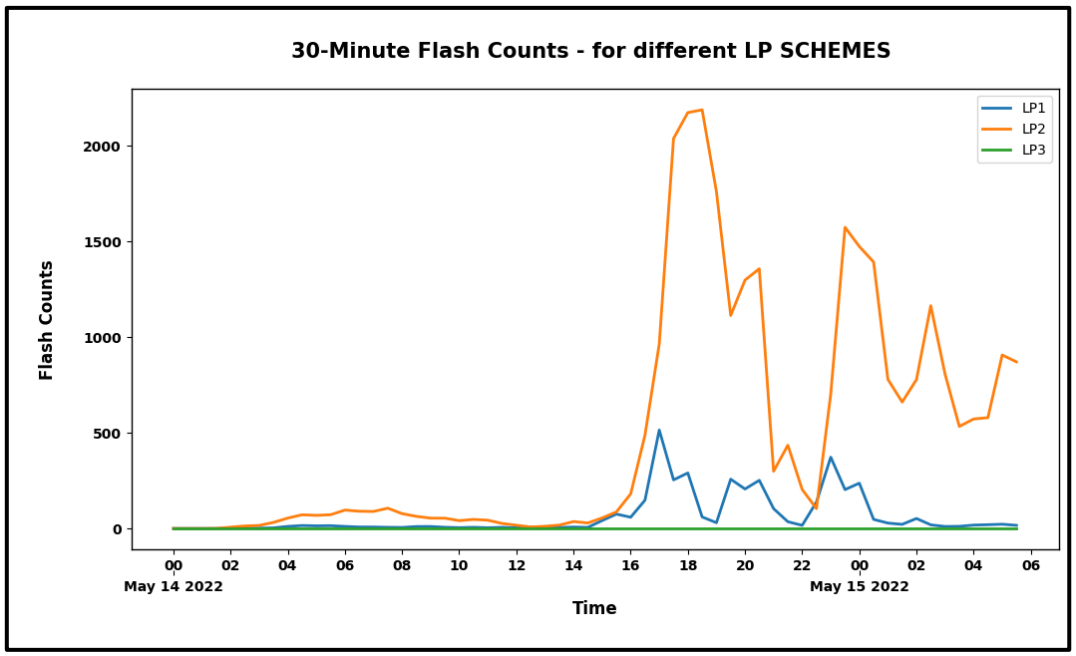

Figure 11(b): Total flash counts (IC flashes + CG flashes) for different LP schemes

3.3.2 Combination of Lightning (LP) and Cumulus (Cu) parameterisation:

Cumulus schemes parameterize sub grid scale effects of shallow and deep convective clouds. Resolution of less than 3 km, cumulus parameterization can be turned off, since the microphysics scheme itself can resolve convection for this resolution.

Resolutions of 3 km < dx, dy < 10 km are called Gray zones where it is considered too coarse for cloud parameterization and potentially too fine to turn on cumulus parameterization. Therefore, it is recommended to test the model performance by turning it on and turning it off for the 3 km < resolution < 10 km.

However, many recent studies pointed out that turning on CU in the Gray zones improves the accuracy. In our study we used both the option to see the variability in simulating lightning.

The Kain-Fritsch (KF) cumulus scheme (Cu Option 1) has been shown to outperform other cumulus schemes (Baki et al., 2021).

3.3.3 Microphysics parameterisation (MP):
(in combination with LP and Cu parameterisation Schemes)

Microphysics parameterization (MP), resolves cloud and precipitation processes, and few schemes account for ice and mixed phase processes too. MP schemes provide atmospheric heat and moisture tendencies to the model and non-convective/resolved scale rainfall at the surface. It considers many different microphysical processes and formation of different particles (mass variables and number variables).

Figure12 represents simulated lightning using two different lightning parameterization (LP) schemes (LP1 and LP2), two cumulus parameterization (CU) schemes ([CU1 : Kain-Fritsch] and [CU2 : Multi Kain-Fritsch]), and seven microphysics (MP) schemes, along with their ensemble mean and spread.

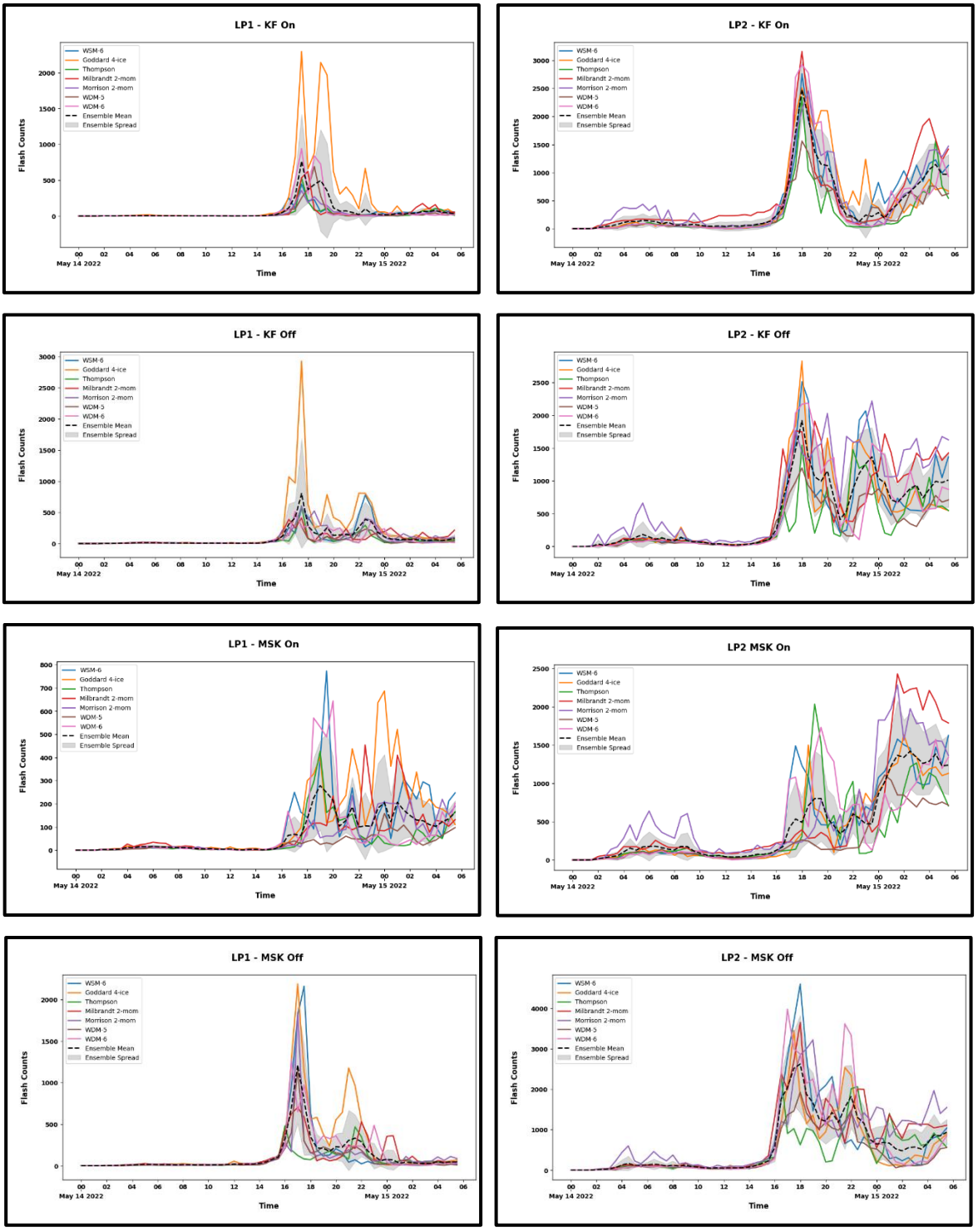

Figure 12: 30-minute simulated output of various parameterisation combinations of the WRF model

The LP1-KF_{on} and LP1-KF_{off} schemes generally produced lower lightning flash amplitudes, with most MP combinations displaying either single peaks or small secondary peaks.

In contrast, the LP1-MSK_{on} scheme exhibited random variability across different MP combinations, whereas LP1-MSK_{off} showed more systematic dual peaks, resembling the observed lightning pattern more closely. On the other hand, the LP2 schemes generated higher lightning flash counts overall.

However, there was significant variation in the temporal evolution depending on whether KF $_{on/off}$ and MSK $_{on/off}$ were applied. When KF/MSK was turned ON in the Gray zone, the dissipation of the secondary peak was poorly represented or delayed by a few hours. Similarly, when KF/MSK was turned OFF in the Gray zone, the secondary peak followed a dissipating pattern but remained at a higher magnitude. These trends were observed across almost all MP schemes in combination with LP2. Overall, LP2 schemes perform better than LP1 in both magnitude and temporal trends

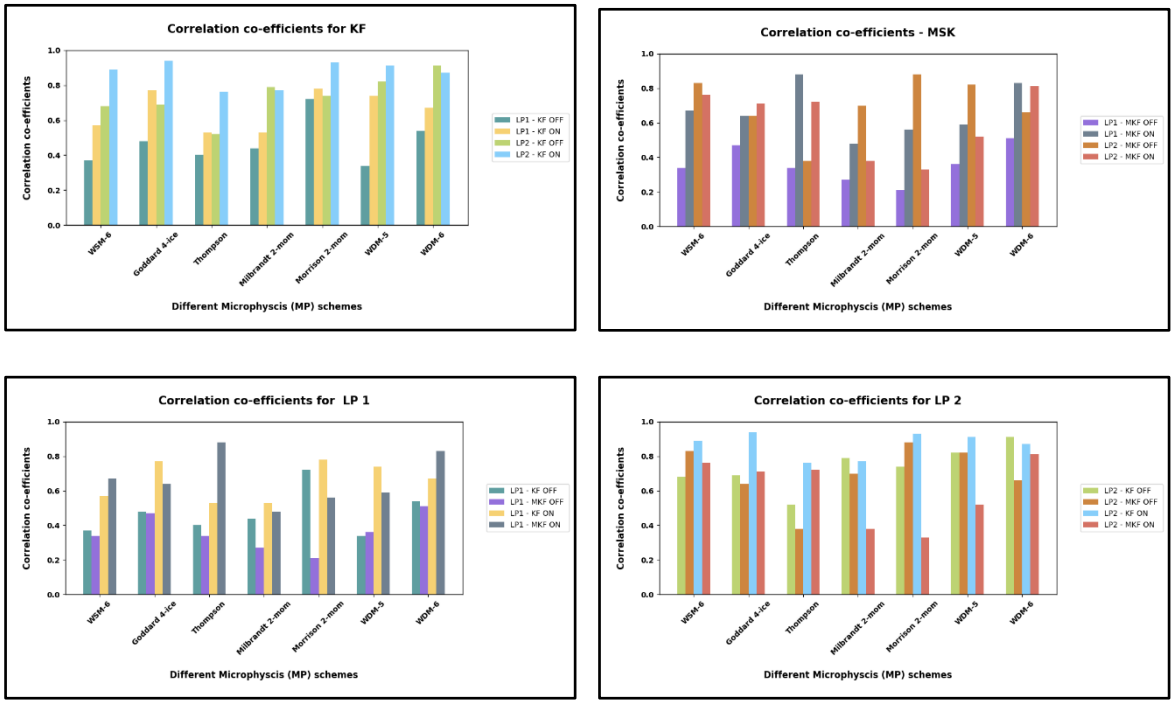

Figure 13: Bar graph showing Correlation coefficient values for different LP and CU schemes and MP schemes with the observed flash counts

It has been found that LP2 schemes perform better than LP1 schemes for any combination of MP schemes. Though LP2 schemes perform better, we wanted to test its performance in combination with various microphysics schemes. Therefore, LP1 and LP2 have been tested with popular seven microphysics schemes (Two Single-moment schemes: WSM-6, Goddard 4-ice, Four Double-moment schemes: Thompson, Milbrandt double-moment, Morrison double-moment, WDM-5 and WDM-6). The correlation coefficients of the different MP schemes for different Cu schemes are shown in Figure 13.

Among the LP2 - MP combinations, double moment schemes (except Thompson) perform better than single moment schemes (Figure 13). More clear understanding of these analysis can be interpreted with the Taylor diagram which is discussed in the nest section

3.4 Performance analysis using Taylor Diagram:

A Taylor diagram is a graphical tool used to evaluate and compare the performance of models by simultaneously displaying three statistical metrics: Correlation Coefficient, Root Mean Square Difference and Standard deviation. In a Taylor diagram, observations are typically represented by a reference point on the x-axis. Model results are plotted as points, with their distance from the reference indicating the RMSE. The angle from the x-axis represents the correlation coefficient, while the radial distance from the origin shows the standard deviation. (Refer Section 2.3.3 for more details about the calculations). This allows for a quick visual comparison of multiple models to determine which performs best in terms of accuracy and variability.

The Taylor diagram showing the performance of all the studied 56 combination of parameterisation schemes is shown in Figure14. Figure 15 shows Taylor diagram for each parameterisation classification. Any combination of Parameterisation schemes with LP1 has very less correlation coefficient and higher Standard deviation. Any Cumulus and Microphysics schemes with LP2 combination performs better than LP1 combination. Among the LP2 combinations, turning on the KF for the innermost domain and turning off MSK for the innermost domain performs better than turning off the KF and Turning on MSK schemes.

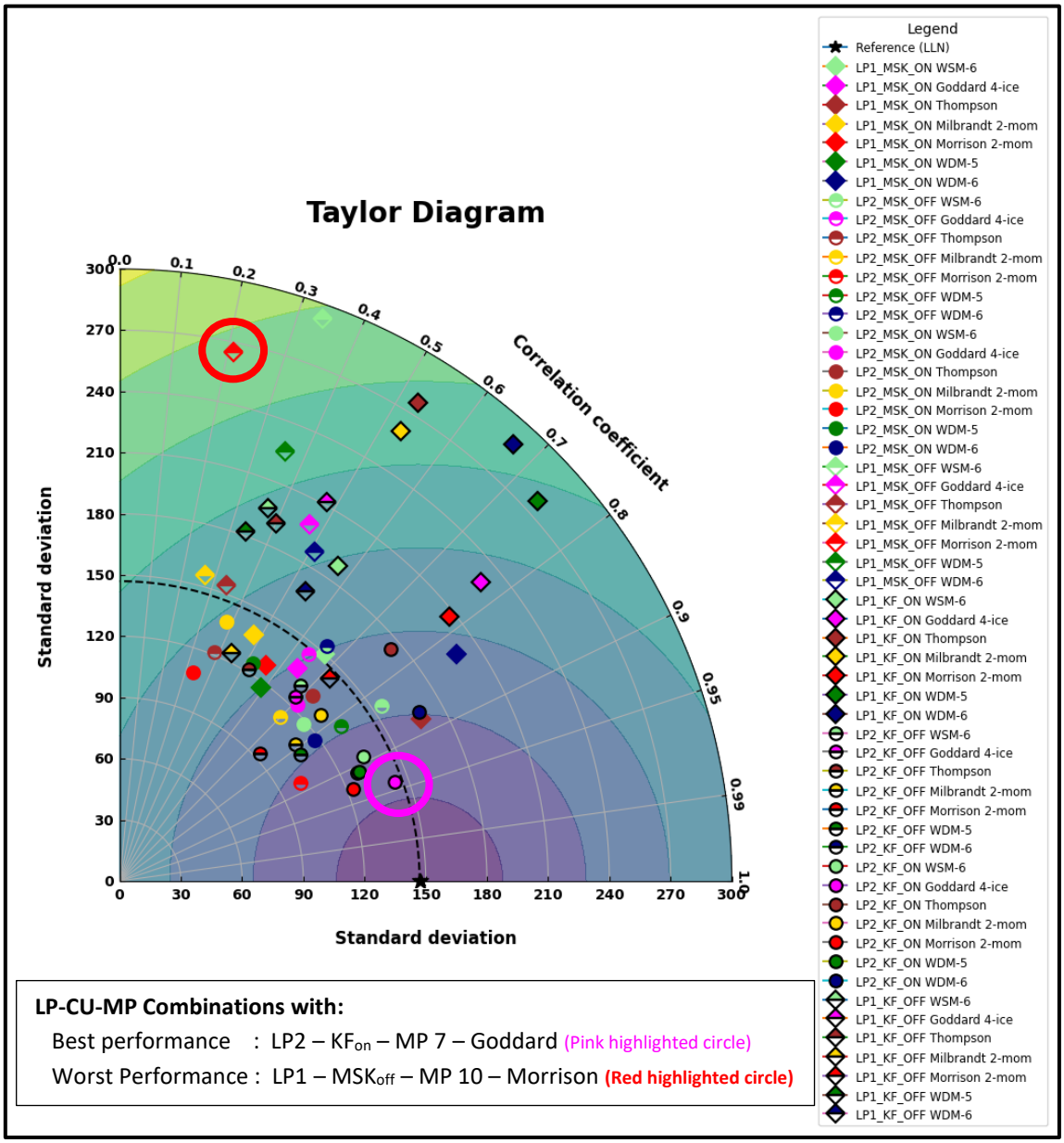

Figure 14: Taylor diagram illustrating the performance of 56 model runs using various combinations of parameterizations (6 MP, 2 Cu, 2 LP schemes)

For better differentiation, the Taylor diagrams are separated for LP1 and LP2 (Figure 15), consistently highlighting the superior performance of LP2, as discussed earlier. This indicates that enabling KF in the Gray zone improves lightning simulations in the region. In case of using MSK in the Gray zone, turning it off for the innermost domain for the Gray zone has better performance.

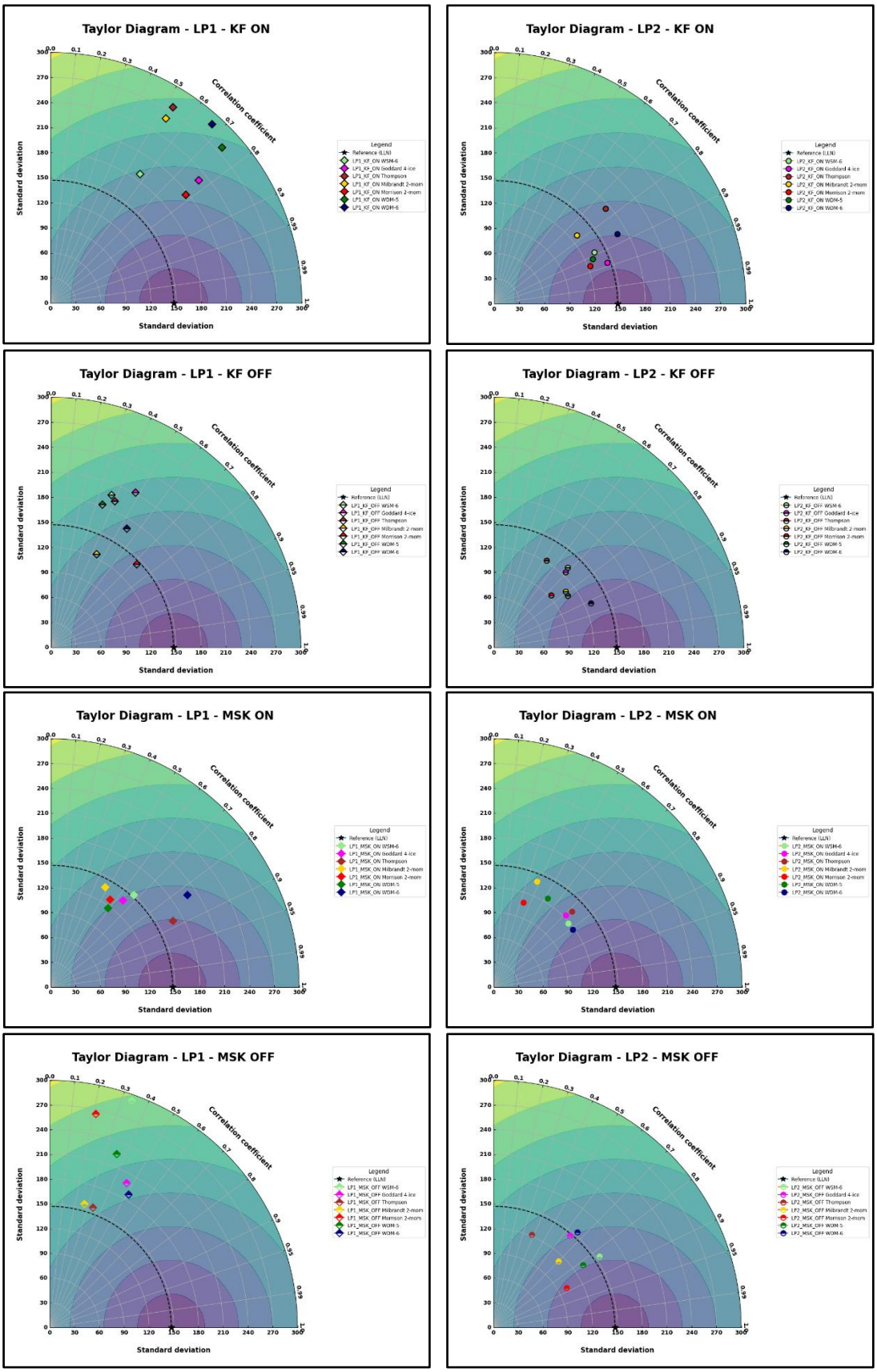

Figure 15: Taylor diagrams depicting the performance of the parameterisation schemes combinations of each category

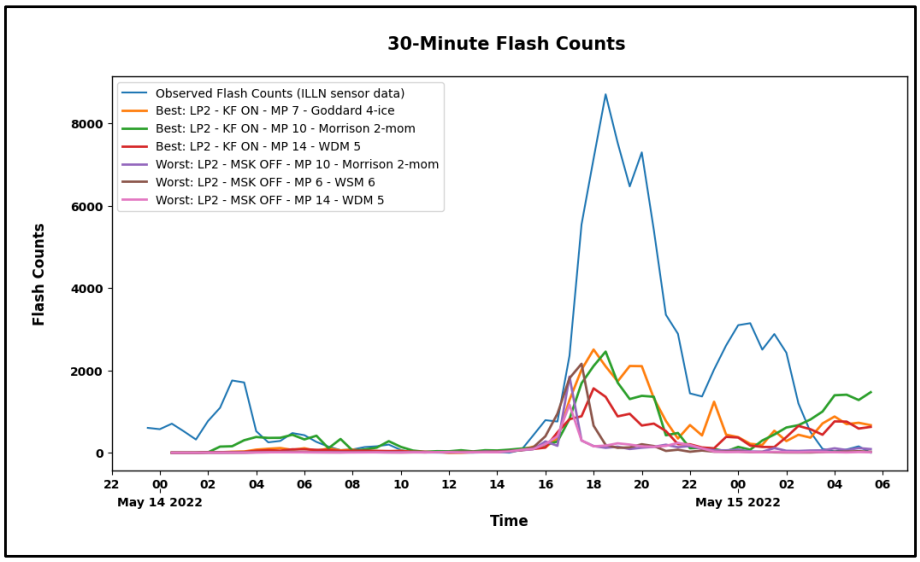

Figure 16 (a): 30-minute Observed and Model simulated Flash counts for three best performing combination schemes and three worst performing combination schemes

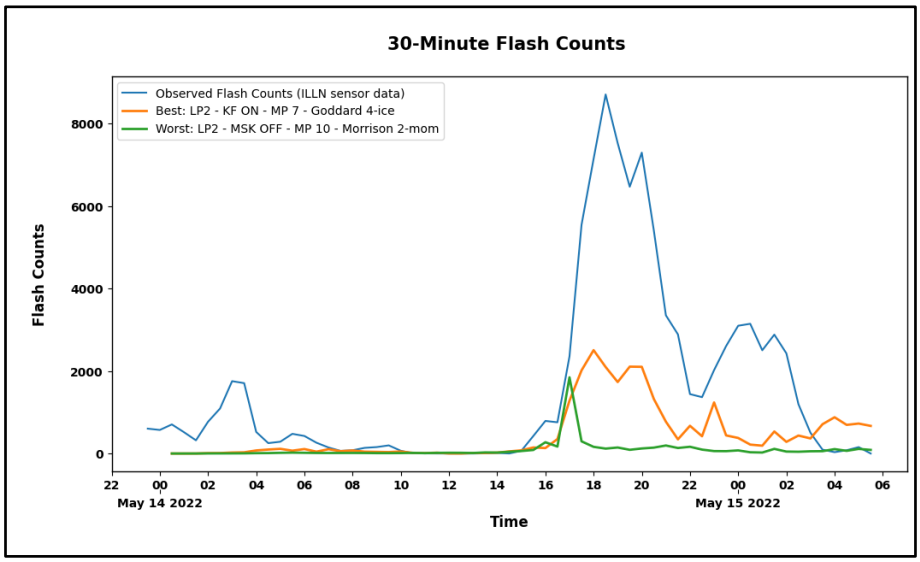

Figure 16 (b): 30-minute Observed and Model simulated Flash counts for the best performing combination schemes and the worst performing combination schemes

The best performing combination schemes though underestimates the observed flash counts, but it can capture the trend and timing of observed flash counts (Figure 16 (a), (b)). The worst performing combination schemes severely underestimates the observed flash counts and cannot the capture the trend and timing of the thunderstorm (too early form the actual thunderstorm event).

3.5 Vertical Profiles of various model parameters:

To understand the possible reasons behind the performance of different schemes, we analysed the vertical representation of microphysical properties for various schemes. Due to the unavailability of observational data for direct comparison with model-derived mixing ratios, we compared the vertical profiles of key mixing ratios (such as water vapor, cloud, and ice), reflectivity profiles as well as the thermodynamical profiles from the best-performing scheme against the worst-performing one.

This comparison highlights the differences in their microphysical representations, providing insights into why certain schemes perform better and how closely they align with observational trends

The best combination is LP2 – KF_{on} – MP 7 - Goddard and the worst performing combination if LP1 – MSK_{off} – MP 10 - Morrison.

3.5.1 Vertical profiles of Convective parameters:

(a) CAPE:

The CAPE profiles for both the best- and worst-performing combinations remain similar throughout the different stages of the thunderstorm event, indicating that the large-scale thermodynamic conditions driving convection are well captured across schemes. (Figure 17 (a)).

This suggests that differences in model performance are not due to variations in atmospheric instability but rather arise from discrepancies in microphysical processes, cloud dynamics, and precipitation formation.

While CAPE governs the potential for convection, the actual storm evolution depends on how each scheme handles moisture, updraft strength, and phase changes within the cloud system.

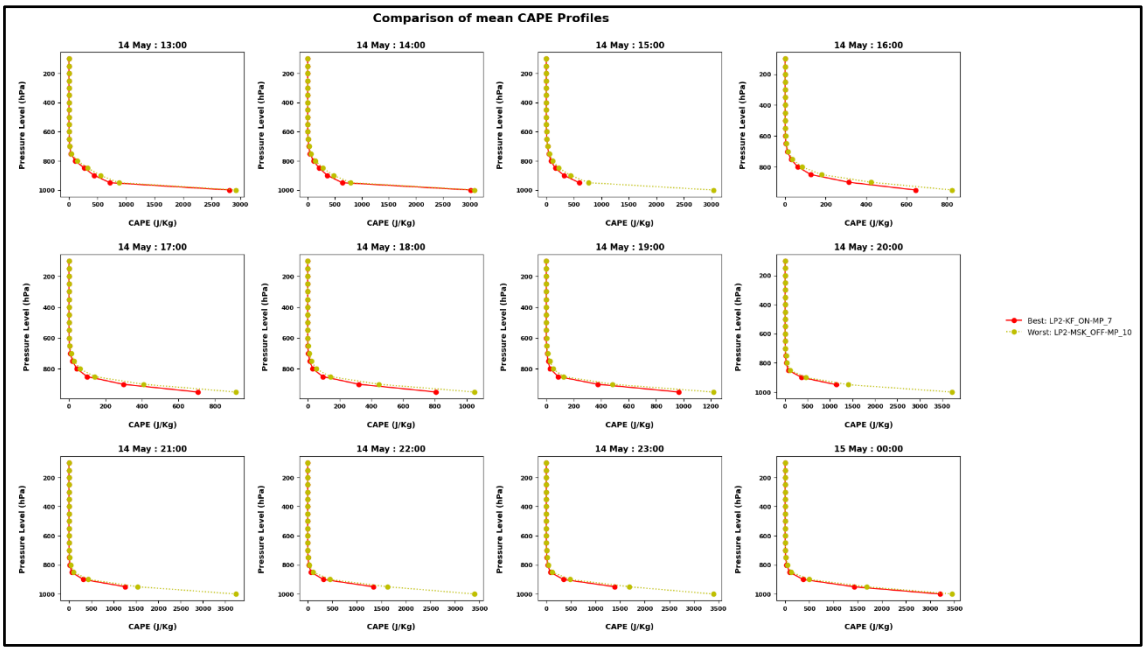

Figure 17 (a): Vertical Profile of Mean CAPE

(b) CINE:

Like CAPE, CINE profiles for both the best- and worst-performing combinations remain similar throughout the different stages of the thunderstorm event, suggesting that the inhibition to convection is consistently represented across schemes

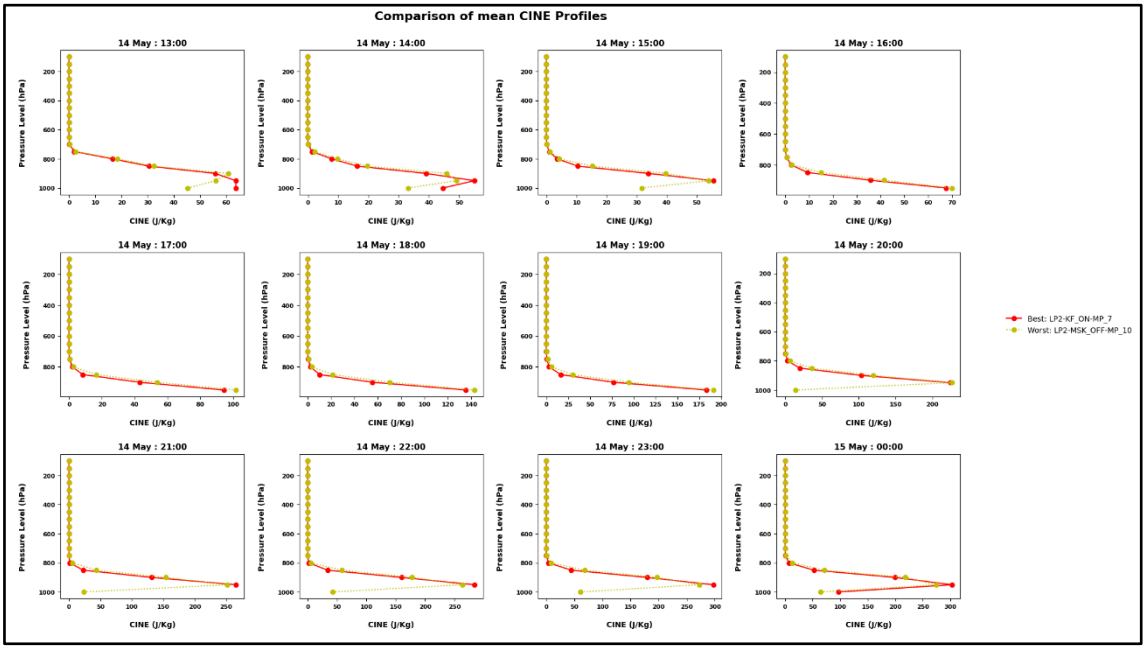

Figure 17 (b): Vertical Profile of Mean CINE

(c) Relative Humidity, Temperature, Wind Speed, LCL, and LFC:

The profiles of Relative Humidity, Temperature, Wind Speed, Lifting Condensation Level (LCL), and Level of Free Convection (LFC) for both the best- and worst-performing combinations remain similar throughout the different stages of the thunderstorm event.

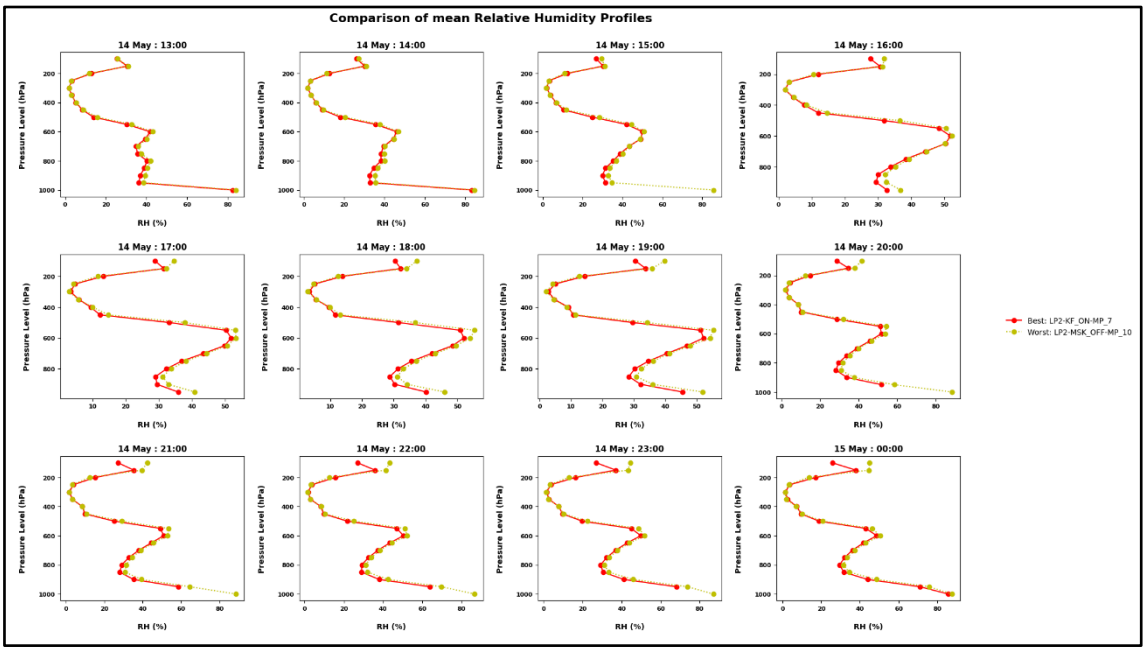

Figure 17 (c): Vertical Profile of Mean Relative Humidity

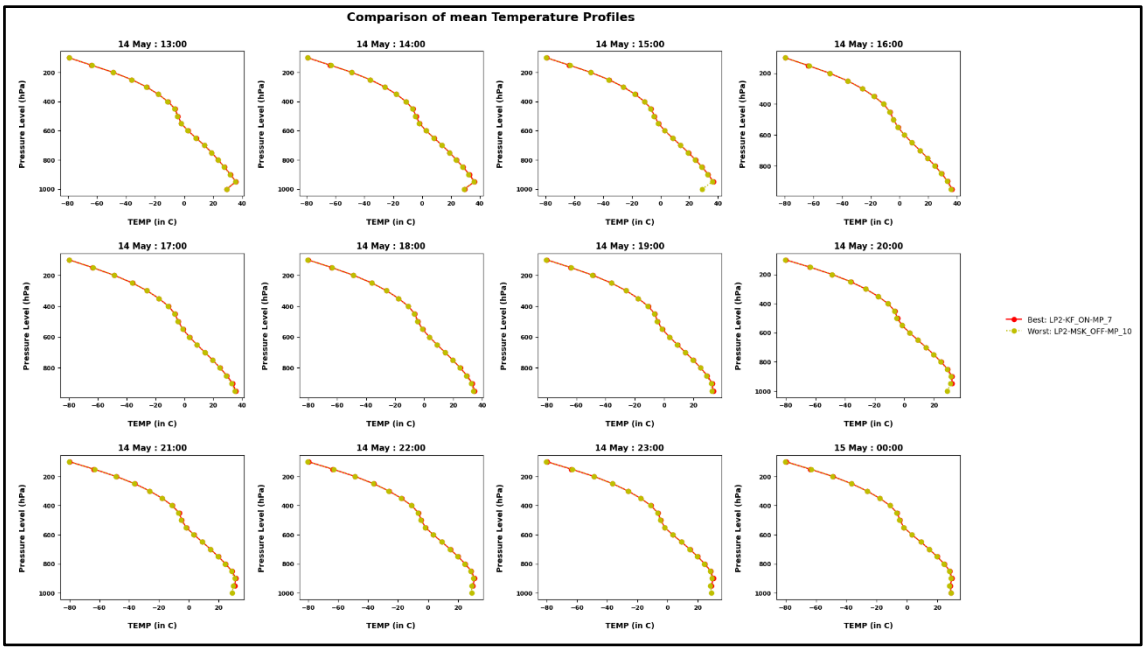

Figure 17 (d): Vertical Profile of Mean Temperature

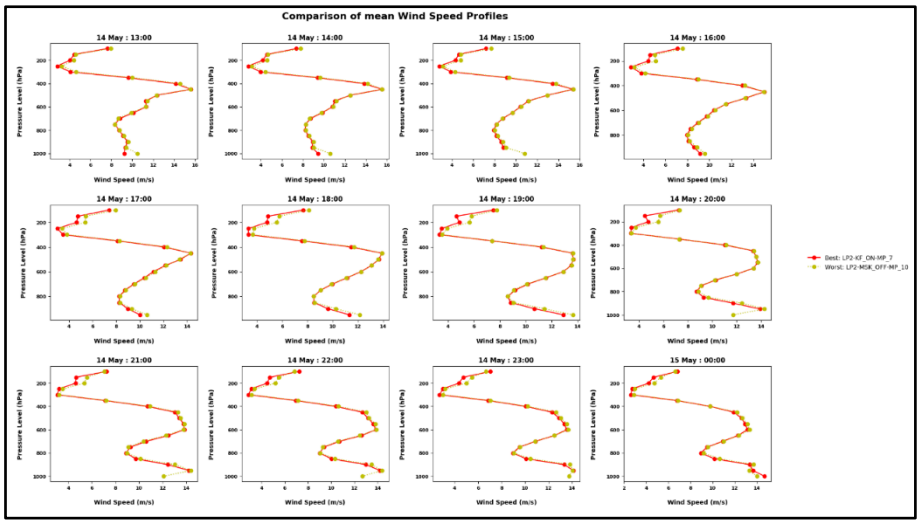

Figure 17 (e): Vertical Profile of Mean Wind Speed

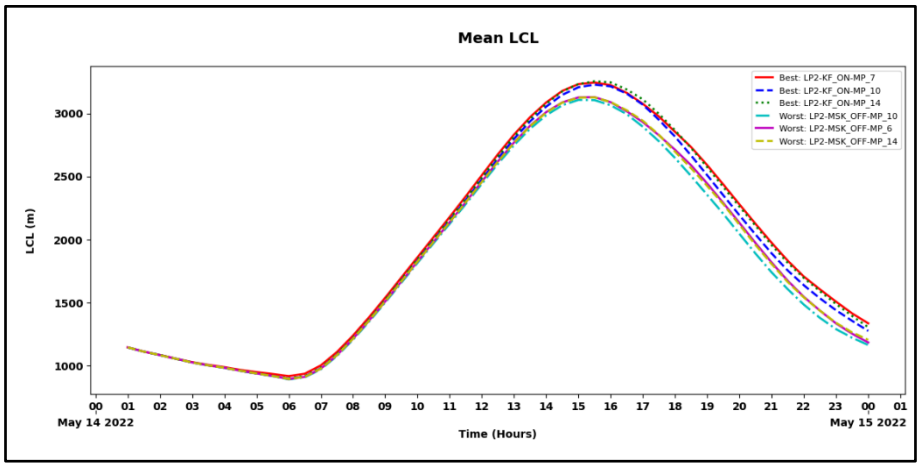

Figure 17 (f): Vertical Profile of Mean LCL

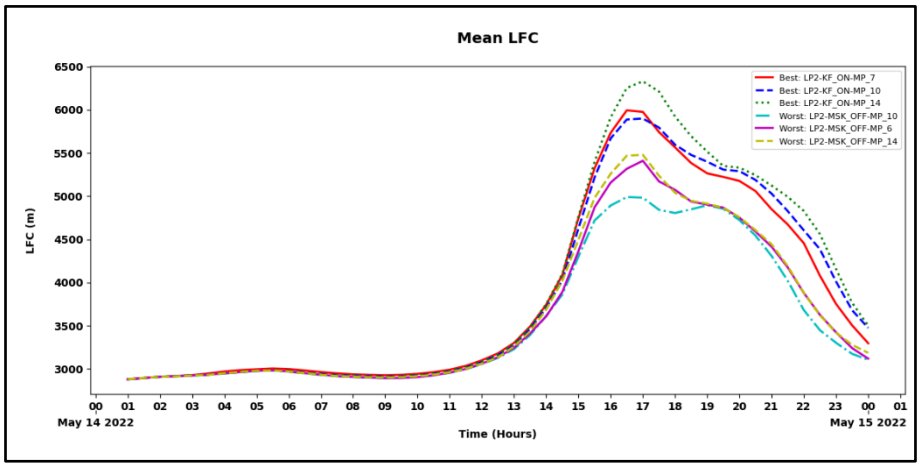

Figure 17 (g): Vertical Profile of Mean LFC

Convective parameters	Initial stage	Mature stage	Dissipating stage	Remarks
CAPE	Have been simulated consistent and similar with each other			The differences in model performance are not due to large-scale thermodynamic parameters
CINE				
Relative humidity				
Temperature				
Wind speed				

Table 4: Summary of the vertical profiles of the convective parameters for different stages of the Thunderstorm

3.5.2 Vertical profiles of Microphysical parameters:

a) Reflectivity:

During the Initial stage of the thunderstorm, both parameterisation combination performs similar with a little differentiation in the lower levels. But during the active thunderstorm stage, the worst performing scheme underestimates the reflectivity values in the middle troposphere leading to its poor performance accuracy.

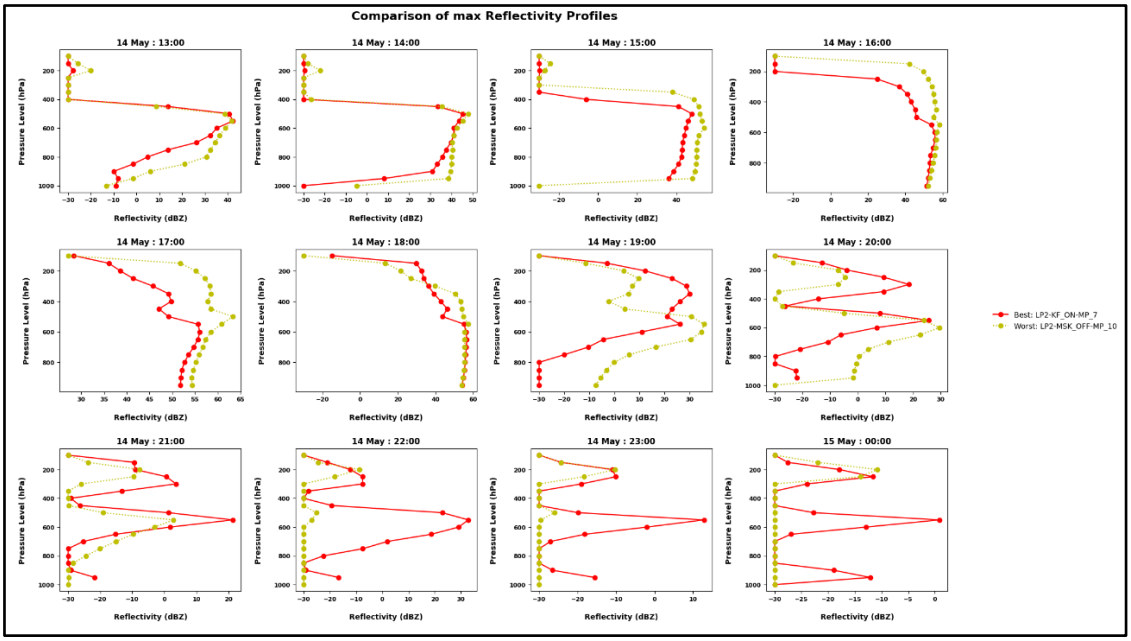

Figure 18 (a): Vertical Profile of Mean Reflectivity

b) Water Vapour Mixing Ratio:

The water mixing ratio for both the best- and worst-performing scheme combinations remains relatively similar throughout the different stages of the thunderstorm event (Figure 18 (b)). This suggests that the overall representation of water vapor in the model does not significantly differ between these schemes.

During the initial development phase, both sets of schemes exhibit comparable moisture availability in the lower and mid-troposphere, which is crucial for cloud formation and convective initiation.

As the storm matures, the vertical distribution of water vapor remains largely consistent, indicating that both scheme groups capture the fundamental moisture transport processes reasonably well.

Even during the dissipation phase, the differences in water vapor mixing ratios remain minimal, suggesting that the primary distinctions in scheme performance may arise from other microphysical processes, such as cloud and ice phase interactions, rather than from water vapor representation alone.

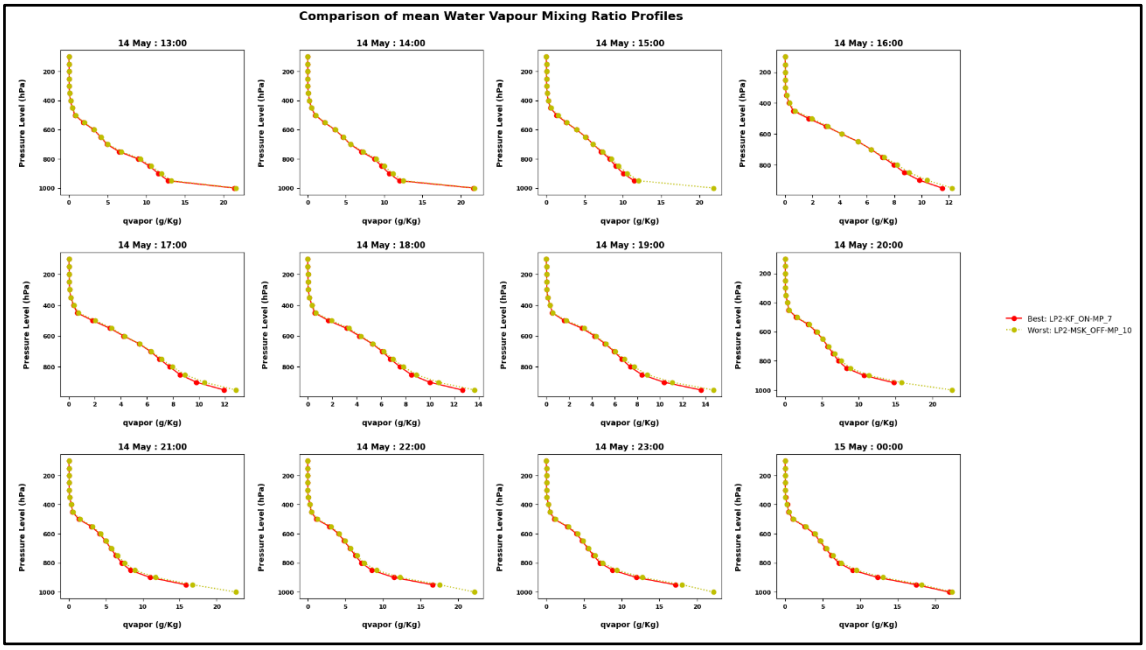

Figure 18 (b): Vertical Profile of Mean Water Vapour Mixing Ratio

c) Cloud Water Mixing Ratio:

The worst-performing combination consistently overestimates the cloud water mixing ratio throughout the various stages of the thunderstorm lifecycle. This overestimation is particularly pronounced during the mature phase of the storm, when convective activity is at its peak. (Figure 18 (c)).

During active thunderstorm conditions, the excessive cloud water content suggests that these schemes may be inefficient in converting cloud droplets into precipitation, leading to an unrealistic buildup of cloud water. Such overestimation can have multiple implications for model performance. First, it may indicate an underrepresentation of auto conversion and accretion processes, which are responsible for the formation of raindrops from cloud droplets. Second, an excessive amount of cloud water can impact latent heat release, altering the thermodynamic profile and potentially leading to biases in updraft strength and storm intensity. Third, the overestimation can affect cloud radiative properties, which in turn influence surface energy fluxes and atmospheric stability.

Ultimately, this overprediction of cloud water mixing ratio reduces the accuracy of the scheme, as it deviates significantly from expected cloud microphysical behavior, leading to errors in precipitation output and storm dynamics.

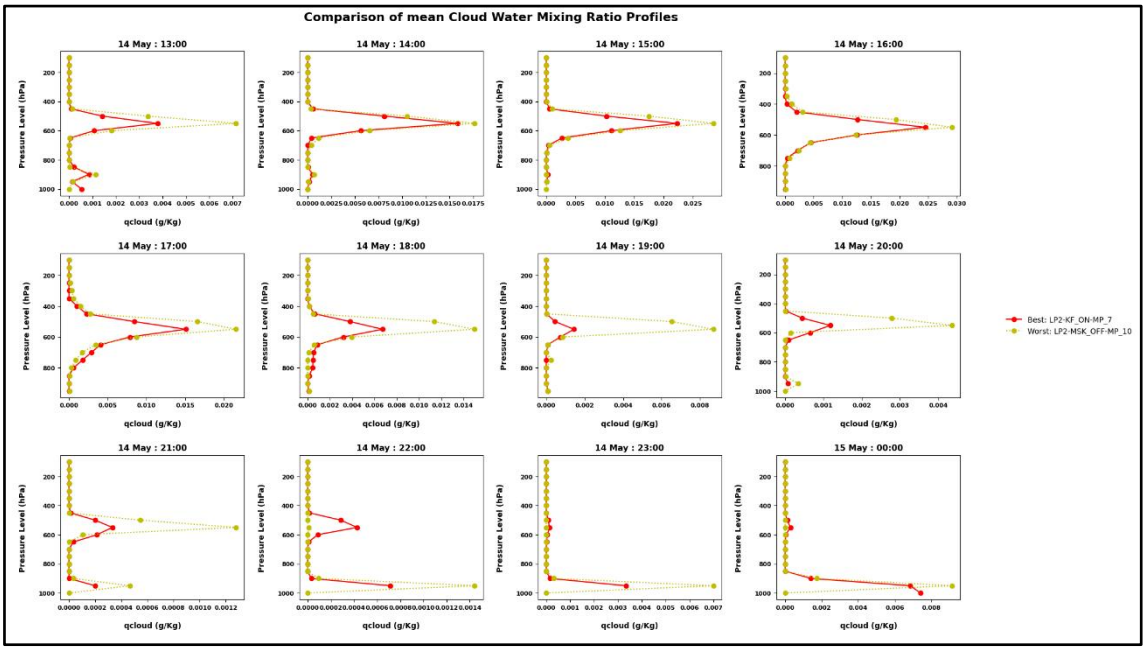

Figure 18 (c): Vertical Profile of Mean Cloud water Mixing Ratio

d) Rain Water Mixing Ratio:

The worst-performing combination exhibits an early overestimation of the rainwater mixing ratio during the initial stages of the thunderstorm, suggesting excessive rain formation before the storm fully matures. However, it underestimates rainwater content in the later stages, likely due to inefficient precipitation processes or excessive evaporation. (Figure 18 (d)).

This misrepresentation affects the storm's overall evolution, leading to inaccuracies in capturing thunderstorm intensity, particularly in peak convective activity and rainfall distribution. The inaccurate rainwater mixing ratio in the worst-performing combination likely results from inefficient microphysical conversions, excessive early autoconversion of cloud droplets, and weak accretion processes, leading to initial overestimation and later underestimation. Overestimated cloud water, excessive evaporation, or premature rainout further contribute to these biases. Misrepresentation of updrafts and downdrafts disrupts rainwater distribution, while errors in ice-phase processes, such as melting of graupel and snow, impact precipitation formation.

Additionally, incorrect latent heat feedback weakens convection, preventing the scheme from accurately capturing thunderstorm intensity.

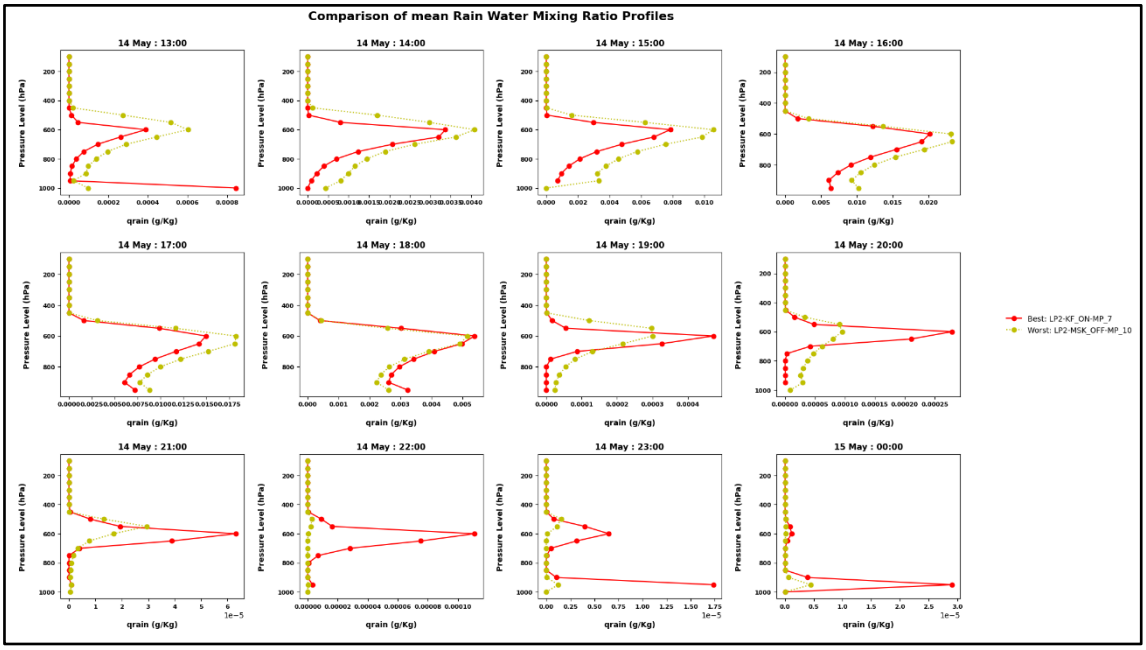

Figure 18 (d): Vertical Profile of Mean Rain Water Mixing Ratio

e) Ice Water Mixing Ratio:

The worst-performing combination exhibits an inconsistent representation of ice water mixing ratio, overestimating it during the early stages of the thunderstorm, underestimating it during peak convective activity, and overestimating it again in the later stages. (Figure 18 (e)).

The initial overestimation suggests excessive ice nucleation or inefficient ice-to-liquid conversion, while the underestimation during the active phase indicates a weak representation of ice growth processes such as riming and aggregation.

The later overestimation may result from delayed ice sedimentation or excessive depositional growth, leading to inaccuracies in storm evolution and precipitation formation.

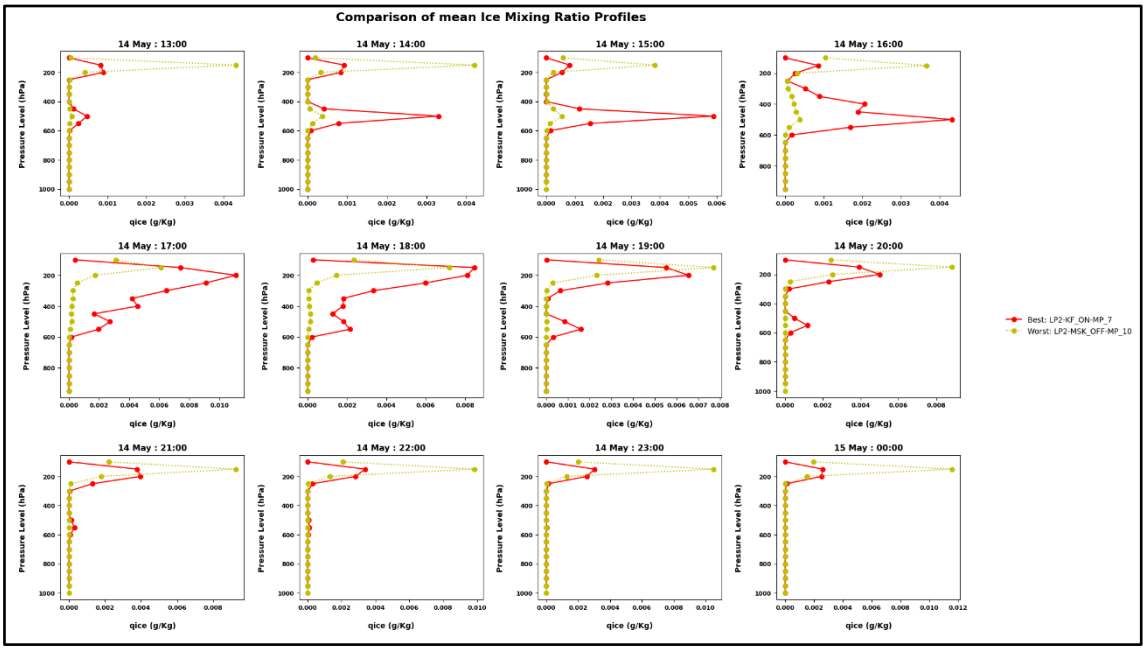

Figure 18 (e): Vertical Profile of Mean Ice Water Mixing Ratio

f) Snow Mixing Ratio:

The worst-performing combination shows an inconsistent snow mixing ratio, overestimating it in the early stages, underestimating it during peak thunderstorm activity, and overestimating it again in the later stages. (Figure 18 (f)).

The initial overestimation suggests excessive snow formation due to inefficient conversion of cloud ice and supercooled water. The underestimation during the active phase indicates weak aggregation and riming processes, leading to insufficient snow production. The later overestimation may result from delayed melting or excessive depositional growth, causing discrepancies in precipitation formation and storm evolution

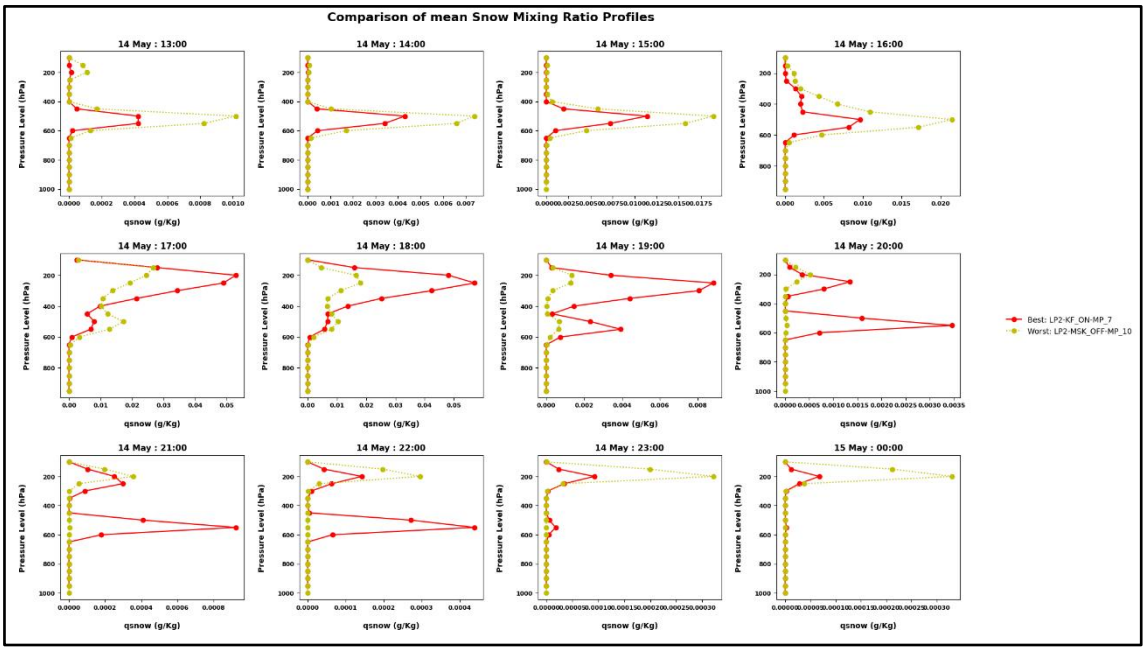

Figure 18 (f): Vertical Profile of Mean Snow Mixing Ratio

g) Graupel Mixing Ratio:

The worst-performing combination overestimates the graupel mixing ratio during the early stages of the thunderstorm, likely due to excessive riming or inefficient conversion of graupel to other hydrometeors. (Figure 18 (g)).

However, in the later stages, it severely underestimates graupel content, suggesting weak graupel production or excessive melting and fallout, leading to an inaccurate representation of storm dynamics.

This misrepresentation affects the overall latent heat release, weakening convection and failing to capture thunderstorm intensity.

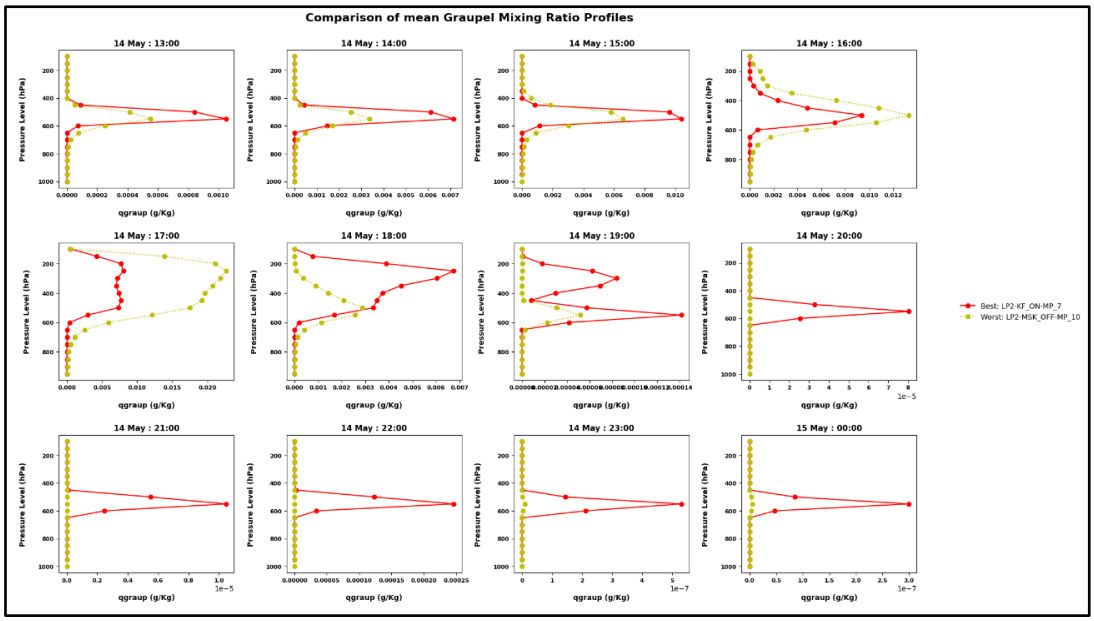

Figure 18 (g): Vertical Profile of Mean Graupel Mixing Ratio

Hydro-meteors	Initial stage	Mature stage	Dissipating stage	Remarks
Water Vapor	Have been simulated consistent and similar with each other			No issues
Cloud water	Similar	Severe Over estimation	Severe Over estimation	Inefficient Auto conversion and Accretion process
Rain water	Over estimation	Under estimation	Severe Under estimation	Early Auto conversion and later Weak Accretion process
Ice water	Over & Under estimation	Over & Under estimation	Severe Over estimation	Excessive ice-nucleation , Inefficient riming process
Snow	Severe Over estimation	Severe Under estimation	Over & Under estimation	Inefficient Riming and Aggregation
Graupel	Over estimation	Severe Under estimation	Severely Under estimation	Early Excessive Riming, later excessive melting and fallout

Table 5: Summary of the vertical profiles of the microphysical parameters for different stages of the Thunderstorm

From the table 5, it is clear that the differences in model performance are not due to large-scale thermodynamic or moisture transport processes but rather stem from the representation of the microphysical processes

In particular,

1. **Auto conversion process** (cloud droplets → Rain droplets)
2. **Riming process (**process in which ice particles gather liquid droplets, causing them to freeze instantly upon contact

3.6 Skew-T Diagram:

(a) Wyoming Sounding Data:

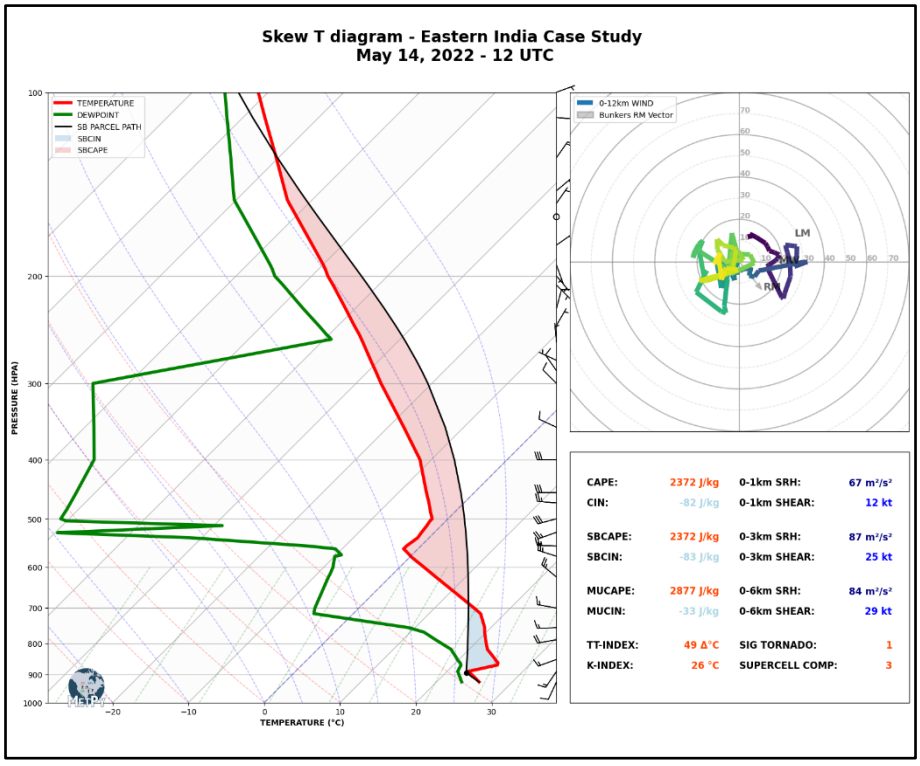

Figure 19: Skew T Diagram of the Wyoming Sounding data (May 14, 2022 - 12 UTC) for the Thunderstorm case study

For the simulation case, atmospheric sounding data from the University of Wyoming was used to analyse thermodynamic conditions, with key parameters computed using the Skew-T Log-P diagram (Figure 19).

The Convective Available Potential Energy (CAPE) was found to be 2372 J/kg, indicating the buoyant energy available for convection, while the Convective Inhibition (CINE) was 82 J/kg, representing the energy needed to overcome atmospheric suppression.

The Lifting Condensation Level (LCL), marking the height where an air parcel becomes saturated, was at 894 hPa, and the Level of Free Convection (LFC), where the parcel becomes positively buoyant, was at 688 hPa.

The Equilibrium Level (EL), indicating the storm's vertical extent, was observed at 126 hPa. These parameters collectively describe the thermodynamic environment influencing thunderstorm development in the simulation case.

(b) WRF best performing scheme combination:

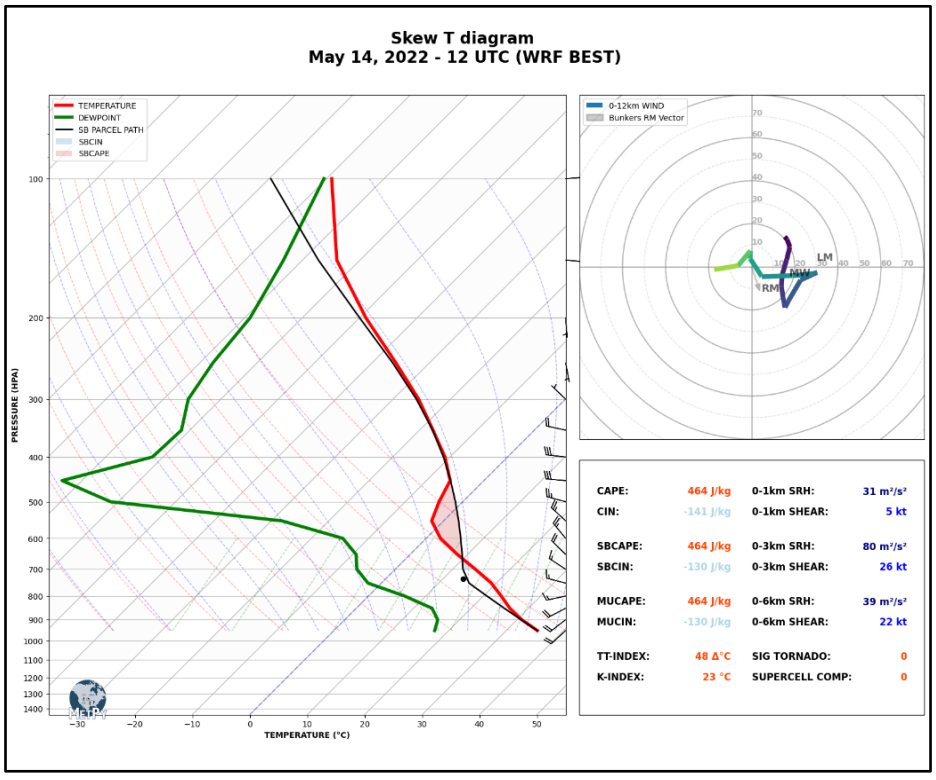

Figure 20: Skew T Diagram of the WRF best performing scheme combination (LP2 - KF_{on} – MP 10 Morrison) (May 14, 2022 - 12 UTC) for the Thunderstorm case study

We computed the thermodynamic parameters from the model simulation (best performing) to analyse the atmospheric conditions associated with the thunderstorm event. Figure 20 represents the vertical profiles of key thermodynamic indices, providing insights into atmospheric stability and convection.

From the simulation, we found that the Convective Available Potential Energy (CAPE) was 464 J/kg, indicating the buoyant energy supporting deep convection, while the Convective Inhibition (CINE) was 141 J/kg, representing the resistance to convection.

The Lifting Condensation Level (LCL) was located at 734 hPa, marking the altitude where lifted air parcels became saturated. The Level of Free Convection (LFC) was at 664 hPa, where air parcels gained positive buoyancy, and the Equilibrium Level (EL) was at 438 hPa, defining the storm's vertical extent.

These findings highlight the thermodynamic environment favouring thunderstorm development in the simulation case. From the model simulation, we found lower values of the thermodynamic parameters compared to observations.

This discrepancy may be due to the areal averaging of the model-derived profiles, which can smooth out localized convective features and reduce peak values.

Another possible reason is a lead-lag effect in the WRF simulation relative to observations, meaning the exact timing of convection in the model may not align perfectly with the observed event.

Such timing differences can impact the computed thermodynamic indices, leading to variations in CAPE, CINE, LCL, LFC, and EL compared to the observational sounding.

4. CONCLUSIONS:

The selection and tuning of parameterization schemes, particularly for microphysics (MP), cumulus (Cu), and lightning (LP) processes, play a critical role in enhancing model performance and accuracy. A total of 56 combinations of various MP, Cu and LP schemes were studied (Different combinations of 2 LP, 2 Cu, 7 MP schemes).

While CU schemes are often disabled at resolutions below 3 km, their effectiveness in the 3–10 km 'Gray zone' is debated. Recent studies suggest enabling CU in this Gray zone enhances model accuracy. This study tests both options to assess variability in lightning simulations.

1. Model Performance:

- The Kain-Fritsch (KF) cumulus scheme turned on for the innermost domain of the WRF model is found to outperform others.
- Microphysics, governing cloud and precipitation processes, also plays a crucial role. Testing seven MP schemes with LP1 and LP2 shows that LP2 generally produces higher flash counts and better temporal trends, particularly with double-moment MP schemes (except Thompson).

2. Quantifying the model performance - Taylor diagrams shows that

- LP2 schemes based on Cloud top height performs better than LP1 schemes based on maximum updraft
- LP2 – KF_{on} combination has higher model performance than other combinations. Whereas, LP1 combinations show lower correlation and higher standard deviation with any combination of MP schemes.
- The Overall best-performing LP-Cu-MP combinations were LP2-KF_{on}-Goddard 4-ice, LP2-KF_{on}-Morrison 2-mom, LP2-KF_{on}-WDM5, LP2-KF_{off}-WDM6, achieving correlation coefficients values of 0.94, 0.93, 0.91, and 0.91 with observed flash counts respectively.

3. To identify the underlying causes for the performance gap between different parameterisation scheme in predicting the lightning flash counts

Vertical profiles of various model parameters

To understand the possible reasons behind the performance of different schemes, we analysed the vertical representation of microphysical properties by the best performing scheme combination (LP2 – KF_{on} – MP 7 – Goddard) (correlation coefficient ~ 0.94 with the observed flash counts) and the worst performing scheme combination (LP1 – MSK_{off} – MP 10 – Morrison) (correlation coefficient ~ 0.21 with observed flash counts)

- Thermodynamic properties were consistently simulated across parameterization schemes, but microphysical differences influence accuracy.
- The worst-performing scheme (LP1 – MSK_{off} – Morrison) overestimates cloud water due to inefficient auto conversion and accretion, leading to excessive droplets and weak precipitation formation.
- It also misrepresents ice-phase processes, overestimating ice and snow early and late in the storm while underestimating them at peak convection. The best-performing scheme (LP2 – KF_{on} – Goddard) provides a more balanced representation, improving alignment with observed trends.
- The differences in model performance are not due to large-scale thermodynamic or moisture transport processes but rather stem from microphysical interactions, particularly cloud water retention, precipitation efficiency, and ice-phase dynamics.

These results suggest that large-scale thermodynamic and dynamic conditions remain consistent, but LP and MP schemes influence lightning prediction accuracy. Optimizing riming efficiency, and hydrometeor phase conversions could enhance model accuracy in future simulations.

REFERENCES:

Baki, H., Chinta, S., Balaji, C., & Srinivasan, B. (2021). A sensitivity study of WRF model microphysics and cumulus parameterization schemes for the simulation of tropical cyclones using GPM radar data. *Journal of Earth System Science*, *130*(4). https://doi.org/10.1007/s12040-021-01682-3

Boccippio, D. J., Cummins, K. L., Christian, H. J., & Goodman, S. J. (n.d.). *Combined Satellite-and Surface-Based Estimation of the Intracloud-Cloud-to-Ground Lightning Ratio over the Continental United States*. https://doi.org/10.1175/1520-0493(2001)129%3C0108:CSASBE%3E2.0.CO;2

Brown, K. A., Krehbiel, P. R., Moore, C. B., & Sargent, G. N. (1971). Electrical screening layers around charged clouds. *Journal of Geophysical Research*, *76*(12), 2825-2835. https://doi.org/10.1029/JC076i012p02825

Gish, O. H., & Wait, G. R. (1950). Thunderstorms and the earth's general electrification. *Journal of Geophysical Research*, *55*(4), 473-484. https://doi.org/10.1029/JZ055i004p00473

Rupraj Biswasharma, Manoj A. Domkawale, Rakesh Ghosh, Abhijeet Gangane, N. Umakanth, Sunil Kumar, V. Gopalakrishnan, Sunil D. Pawar, Elizabeth DiGangi, Sachin M. Deshpande, Debajyoti Samanta, Sanjay Sharma, Assessment of the Indian Lightning Location Network (ILLN) using ground-based and satellite observations, Atmospheric Research, Volume 320, 2025, 108069, ISSN 0169-8095, https://doi.org/10.1016/j.atmosres.2025.108069.

Biswasharma, R., Umakanth, N., Pongener, I., Longkumer, I., Rao, K. M. M., Pawar, S. D., Gopalkrishnan, V., & Sharma, S. (2024). Sensitivity analysis of cumulus and microphysics schemes in the WRF model in simulating Extreme Rainfall Events over the hilly terrain of Nagaland. *Atmospheric Research*, *304*. https://doi.org/10.1016/j.atmosres.2024.107393

Gayatri Vani, K., Mohan, G. M., Hazra, A., Pawar, S. D., Pokhrel, S., Chaudhari, H. S., Konwar, M., Saha, S. K., Mallick, C., Das, S. K., Deshpande, S., Ghude, S. D., Domkawale, M., Rao, S. A., Nanjundiah, R. S., & Rajeevan, M. (2022). Evaluation and Usefulness of Lightning Forecasts Made with Lightning Parameterization Scheme Coupled with WRF Model. *Weather and Forecasting*, *37*(3). https://doi.org/10.1175/WAF-D-21-0080.1

Krehbiel, P. R. (1986). The Earth's electrical environment. *The Electrical Structure of Thunderstorms*, 90-113.

Mohan, G. M., Gayatri Vani, K., Hazra, A., Mallick, C., Chaudhari, H. S., Pokhrel, S., Pawar, S. D., Konwar, M., Saha, S. K., Das, S. K., Deshpande, S., Ghude, S., Barth, M. C., Rao, S. A., Nanjundiah, R. S., & Rajeevan, M. (2021). Evaluating different lightning parameterization schemes to simulate lightning flash counts over Maharashtra, India. *Atmospheric Research*, *255*. https://doi.org/10.1016/j.atmosres.2021.105532

Montanyà, J., Soula, S., & Pineda, N. (2007). A study of the total lightning activity in two hailstorms. *Journal of Geophysical Research: Atmospheres*, *112*(D13). https://doi.org/10.1029/2006JD007203

Pawar, V. S., Domkawale, M. A., Bhalwankar, R. V., Gopalakrishnan, V., & Pawar, S. D. (2023). Lightning activity and Convective Available Potential Energy during different phases of Indian summer monsoon season over central region of India. *Meteorology and Atmospheric Physics*, *135*(4). https://doi.org/10.1007/s00703-023-00969-y

Price, C., & Rind, D. (1992). A simple lightning parameterization for calculating global lightning distributions. *Journal of Geophysical Research*, *97*(D9), 9919–9933. https://doi.org/10.1029/92JD00719

Price, C., & Rind, D. (1993). What determines the cloud-to-ground lightning fraction in thunderstorms? *Geophysical Research Letters*, *20*(6), 463–466. https://doi.org/10.1029/93GL00226

Ranalkar, M. R., & Chaudhari, H. S. (2009). Seasonal variation of lightning activity over the Indian subcontinent. *Meteorology and atmospheric physics*, *104*, 125-134. https://doi.org/10.1007/s00703-009-0026-7

Reynolds, S. E., & Neill, H. W. (1955). The distribution and discharge of thunderstorm charge-centers. *Journal of Atmospheric Sciences*, *12*(1), 1-12. https://doi.org/10.1175/1520-0469(1955)012%3C0001:TDADOT%3E2.0.CO;2

Simpson, G. C. (1927). The mechanism of a thunderstorm. *Proceedings of the Royal Society of London. Series A, Containing Papers of a Mathematical and Physical Character*, *114*(768), 376-401. https://doi.org/10.1098/rspa.1927.0048

Simpson, G. C., & Robinson, G. D. (1941). The distribution of electricity in thunderclouds, II. *Proceedings of the Royal Society of London. Series A. Mathematical and Physical Sciences*, *177*(970), 281-329. https://doi.org/10.1098/rspa.1941.0013

Simpson, G. C., & Scrase, F. J. (1937). The distribution of electricity in thunderclouds. *Proceedings of the Royal Society of London. Series A-Mathematical and Physical Sciences*, *161*(906), 309-352. https://doi.org/10.1098/rspa.1937.0148

Stolzenburg, M., Rust, W. D., Smull, B. F., & Marshall, T. C. (1998). Electrical structure in thunderstorm convective regions: 1. Mesoscale convective systems. *Journal of Geophysical Research: Atmospheres*, *103*(D12), 14059-14078. https://doi.org/10.1029/97JD03546

Vonnegut, B. (1955). Possible mechanism for the formation of thunderstorm electricity. *Geophys. Res. Pap*, *42*, 169-181.

Williams, E., Mushtak, V., Rosenfeld, D., Goodman, S., & Boccippio, D. (2005). Thermodynamic conditions favorable to superlative thunderstorm updraft, mixed phase microphysics and lightning flash rate. *Atmospheric Research*, *76*(1-4), 288-306. https://doi.org/10.1016/j.atmosres.2004.11.009

Williams, E. R. (2017). Meteorological aspects of thunderstorms. In *Handbook of Atmospheric Electrodynamics, Volume I* (pp. 27-60). CRC Press.

Wilson, C. T. R. (1921). III. Investigations on lighting discharges and on the electric field of thunderstorms. *Philosophical Transactions of the Royal Society of London. Series A, Containing Papers of a Mathematical or Physical Character*, *221*(582-593), 73-115. https://doi.org/10.1098/rsta.1921.0003

Figure References:

1. Krider, E.P. (2025, March 16). *thunderstorm*. *Encyclopedia Britannica*. https://www.britannica.com/science/thunderstorm
2. https://thegeoroom.co.zw/climatology/rainfall-formation-theories/
3. https://www.faculty.luther.edu/~bernatzr/Courses/Sci123/Chapter12/chargeSeparation.html